Transportation Geotechnics 41 (2023) 101026

Contents lists available at ScienceDirect

Transportation Geotechnics

journal homepage: www.elsevier.com/locate/trgeo

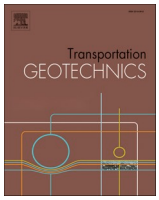

Use of hydraulic radius to estimate the permeability of coarse-grained materials using a new geodatabase

Shuyin Feng [a,b], Daniel Barreto [c], Emőke Imre [d], Erdin Ibraim [e], Paul J. Vardanega [e,*]

[a] Department of Built Environment, Birmingham City University, Birmingham B4 7XG, UK
[b] Formerly Department of Civil Engineering, University of Bristol, Bristol, UK
[c] School of Computing, Engineering and the Built Environment, Edinburgh Napier University, Edinburgh EH10 5DT, UK
[d] EKIK HBM Systems Research Center, Bánki Donát Faculty of Mechanical and Safety Engineering, Óbuda University, Hungary
[e] Department of Civil Engineering, University of Bristol, Bristol BS8 1TR, UK

ARTICLE INFO

Keywords:
Granular soil
Permeability
Hydraulic radius

ABSTRACT

This paper reviews commonly used parameters and prediction models for assessing the permeability of granular soils. Following a review of published models for prediction of soil permeability, a dimensional homogenous transformation model for a-priori estimation of soil permeability was calibrated using a large database (CG/KSAT/7/1278) comprising permeability data for a wide range of granular soils sourced from over 50 publications. The new transformation model requires knowledge of the void ratio and gradation of the material to make estimates of the soil permeability. The prediction accuracy of the calibrated model was then assessed alongside that of other empirical and semi-empirical models also calibrated using CG/KSAT/7/1278. The potential influences of void ratio, key gradation parameters and permeability test type on the prediction accuracy of the proposed model are also examined. The paper shows that while the fitted constants in the proposed transformation model are affected to varying extents by the aforementioned parameters, it does offer reasonable predictions of permeability with only knowledge of the void ratio and material gradation required.

Introduction

Permeability is closely linked to many geotechnical phenomena [1,2]. Information on soil permeability is important for geotechnical design works [3,4], contaminant and waste management [5,6] and performance of energy geo-structures [7]. The intrinsic permeability (K) of granular soils can be obtained by laboratory (or field) testing. However, these tests are often time-consuming and complex to perform (e.g., as discussed in Chapuis [2]). The use of basic soil parameters to give a-priori estimates of K is commonplace, for example, the influence of gradation parameters on the K of granular soils has been widely studied [8–13]. Some of the commonly used prediction models for K (or the coefficient of permeability (k)) have also been reviewed by Mujtaba *et al.* [14].

Table 1 summarises some published empirical and semi-empirical approaches for prediction of K including some recently established transformation models which will be used in the analysis presented in this paper. This paper focuses on saturated soils as for unsaturated soils permeability may be related to the vapour flow e.g. [15].

Model development

Many of the existing predictive models (see Table 1) are either developed based on or analogous to Kozeny-Carman's equation (with the void ratio (e) function and square of the specific surface) or Hazen's formula (with the square of the effective particle size). Notwithstanding the difference in their predictors and forms, both the Kozeny-Carman and Hazen equations can be anticipated from Poiseuille's law [1,36–38] which describes the steady flow through a single straight circular pipe (Eq. (1)):

$$v_{ave} = \frac{\gamma R^2}{8\mu} i \tag{1}$$

where v_{ave} is the average flow velocity in the pipe, R is the radius of the circular pipe (Length), μ is the dynamic viscosity, i is the hydraulic gradient and γ is the unit weight.

Any granular soil mixture can be modelled as an analogous pipe network in solids and then further simplified to a set of pipe bundles. A simplified model for soil K can be obtained by replacing the radius R (Length) of a circular pipe with the equivalent hydraulic radius R_H

* Corresponding author.
E-mail address: p.j.vardanega@bristol.ac.uk (P.J. Vardanega).

https://doi.org/10.1016/j.trgeo.2023.101026
Received 20 March 2023; Received in revised form 26 April 2023; Accepted 11 May 2023
Available online 17 May 2023

Nomenclature

Latin symbols

A	the relative base entropy
A_S	the area of cross section of soil (Length^2)
$AV\%$	the air void percentage in asphalt concrete mixture
B	the normalised entropy increment
b	an exponent
c	a constant
C	composite shape factor
C_H	Hazen empirical coefficient (Length^{-1}.Time^{-1})
$C_{K\text{-}C}$	Kozeny–Carman coefficient
C_U	the coefficient of uniformity
C_Z	the coefficient of curvature
D	the larger sieve size (Length)
d	the smaller sieve size (Length)
D_0	the exact sieve size of which 0% of the soil could pass (Length)
D_{10}	effective particle size for which 10% of the soil is finer (Length)
D_{50}	effective particle size for which 50% of the soil is finer (Length)
d_{eq}	equivalent diameter
D_{min}	minimal measurable particle size (Length)
D_S	effective grain size
e	void ratio
$f(n)$	porosity factor
$f(s)$	pore shape factor
g	gravitational acceleration (Length.Time^{-2})
G_s	specific gravity
H	apparent flow length (Length)
i	hydraulic gradient
k	coefficient of permeability (Length.Time^{-1}) = $K(\gamma/\mu)$
K	intrinsic permeability (Length^2)
$k_{20^\circ C}$	coefficient of permeability at 20 °C (Length.Time^{-1})
k_{ref}	the reference coefficient of permeability value (Length.Time^{-1})
k_{sat}	saturated coefficient of permeability (Length.Time^{-1})
L	length of the hydraulic flow path (Length)
P_{NoD}	percentage by weight of particles retained on the larger sieve
P_{Nod}	percentage by weight of particles retained on the smaller sieve
Q	flow rate (Length^3.Time^{-1})
R	radius of the circular pipe (Length)
R_H	hydraulic radius (Length)
S	the grading entropy
S_0	the base entropy
S_A	specific surface area per unit volume of particles (Length^{-1})
S_r	degree of saturation (%)
S_S	specific surface area per unit mass of particles (Length^2.Mass^{-1})
t	temperature (°C)
v	superficial velocity (Length.Time^{-1})
v_{ave}	average flow velocity in the pipe (Length.Time^{-1})
w/w_L	water content ratio
w	water content
w_L	liquid limit
x	an exponent

Greek symbols

ΔS	the entropy increment
α	a coefficient
β	an exponent
γ	permeant unit weight (Mass. Length.Time^{-2})
μ	dynamic viscosity of the permeant (Mass.Time^{-1}.Length^{-1})
ρ	density of the permeant (Mass.Length^{-3})

Statistical terms

n	number of data points
p	p- value. *The p-value* represents the smallest level of statistical significance that would lead to rejection of the null hypothesis (see [117]). The *p-value* quoted in this paper was calculated using Matlab®
R^2	coefficient of determination
RD	relative deviation = $(100\sqrt{(1-R^2)})$ (see Waters & Vardanega [123] for full definition)
SE	the standard error

(Length) which is often defined as the ratio of the cross-sectional area of the flow passage to the wetted perimeter [1,37,39–42]:

$$K = f(s)f(n){R_H}^2 \tag{2}$$

where $f(s)$ is the pore shape factor, and $f(n)$ is the porosity factor that correlates the average velocity (v_{ave}) in the tube bundle (Eq.1) to the superficial velocity v of the soil structure.

The pore shape factor $f(s)$ was empirically assessed to be approximately 5 for uniform spheres by Carman [23], a range of values (3.4 to 12.81) for different types of porous mediums are reported in subsequent publications (e.g., Mathavan & Viraraghavan [43] and Li & Gu [44]). The pore shape factor depends on both the shape of the grain particles and the tortuosity of the flow channel.

Fair & Hatch [45] reported a series of shape factor values for different particle shapes, ranging from 6.0 to 7.7. The tortuosity of the flow channel quantifies the ratio of the length of the actual hydraulic flow path to the apparent flow length. An estimation of tortuosity could be made using void ratio (e) or porosity (n) [46–49].

The porosity factor is often taken as $\frac{e}{1+e}$ (or n) [1,21,23,38,50]. Baver [51] suggests the infiltration rate of soil depends upon the content of large (non-capillary) pores permitting fluid percolation rather than the total volume of pores. Yokoyama & Takeuchi [52] indicate that a better prediction of K could be achieved with the 'transport porosity' but this is rarely reported. According to Yokoyama & Takeuchi [52] the transport porosity considers only pores that can transmit flow through the entire sample as opposed to ones that come to a dead end within the sample. The e of granular soil is generally less than 1 [36,38,53]. The permeability may be related to the pore-size distribution rather than the macro soil parameters of e and n [54]. The water film that can form around the soil particles should be considered in the estimation of the permeability of unsaturated soils [55].

As both the pore shape function $f(s)$ and the porosity function $f(n)$ depend to some extent on the e parameter, Eq. (2) may be further simplified to:

$$K = a{R_H}^2 e^b \tag{3}$$

where the coefficient a and the exponent b remain undefined and require calibration using assembled databases.

The R_H of the soil can be expressed as $\frac{e}{S_A}$ (e.g., Taylor [1] (p.109)) a similar form can also be found in Ren & Santamarina [56]), Eq. (3) therefore becomes:

Table 1
Summary of empirical and semi-empirical prediction models.

Source	Formulation	Parameters	Applicability
Hazen [16–18]	$k = (0.7 + 0.3t)C_H{D_{10}}^2$	t is the temperature (°C) C_H is the Hazen empirical coefficient (Length^{-1}. Temperature^{-1}) at a water temperature of 10 °C, generally falls between 400 and 1200 as suggested by Hazen [18] D_{10} is the sieve aperture size allows ten percent of the mixture to pass (Length)	$C_U < 5$ 0.1 mm $< D_{10} <$ 3 mm (C_U = the coefficient of uniformity)
Shepherd [19]	$k = cD_{10}^{x}$	c is a constant. x ranges from 1.11 to 2.05, mostly between 1.65 and 1.85.	
Taylor [1]	$k = C\left(\frac{\gamma}{\mu}\right)\left(\frac{{D_S}^2 e^3}{1+e}\right)$	γ is the unit weight of the permeant (Mass.Length^{-2}. Temperature^{-2}) μ is the dynamic viscosity of the permeant (Mass.Length^{-1}. Temperature^{-1}) C is the composite shape factor D_S is the effective grain size	
Chapuis [20]	$k_{sat}(\frac{cm}{s}) = 2.4622(\frac{D_{10}(mm)^2 e^3}{1+e})^{0.7825}$	D_{10} is the sieve aperture size allows ten percent of the mixture to pass (Length) e is the void ratio.	Natural soil, 0.003 mm $\leq D_{10} \leq$ 3 mm; $0.3 \leq e \leq 1$
Kozeny [21], Carman [22,23] (form shown follows Carrier [24])	$k = \left(\frac{\gamma}{\mu}\right)\left(\frac{1}{C_{K-C}}\right)\left(\frac{1}{{S_A}^2}\right)\left(\frac{e^3}{1+e}\right)$	$C_{K\text{-}C}$ is the Kozeny–Carman coefficient, taken to be 5 for uniform spheres by Carman [23] (published $C_{K\text{-}C}$ values can vary from 3.4 to 12.81 for different materials [25]) S_A = specific surface area per unit volume of particles (Length^{-1});	Non-clayey soil
Feng & Vardanega [26,27]	$k_{sat}(\frac{m}{s}) = 1.91 \times 10^{-9}(\frac{w}{w_L})^{4.083}$	w/w_L is the water content ratio w_L is a substitute for the specific surface by mass (S_S) for fine-grained soil (following the work presented in e.g., Farrar & Coleman [28], Muhunthan [29] and Sridharan *et al.* [30]).	Calibrated using fine-grained soil database
Feng *et al.* [31]	$k_{20^\circ C}(\frac{mm}{s}) = 145.47A^{8.90}B^{-2.30}$	A is the relative base entropy. B is the normalised entropy increment. A and B can be calculated following the method described in Feng *et al.* [31], see Lőrincz [32] and Singh [33] for further details on the grading entropy theory.	A coarse-grained soil
Feng *et al.* [34]	$k_{20^\circ C}(\frac{mm}{s}) = 671.83A^{5.59}B^{-1.30}e^{4.58}$		A coarse-grained soil
Feng *et al.* [35]	$\frac{k}{k_{ref}} = AV(\%)^{4.70}S^{10.52}$	$k_{ref} = 1.16 \times 10^{-16}$ mm/s $AV\%$ is the air void percentage in asphalt concrete mixture S is the grading entropy	Calibrated using an asphalt concrete permeability database

$$K = \alpha \frac{e^{\beta}}{{S_A}^2} \tag{4}$$

where, $\beta = b + 2$ and S_A is the specific surface area per unit volume of particles (Length^{-1}) [24], which may be calculated from the particle size distribution [24,37,57].

Chapuis & Légaré [58] proposed a simple method to compute the specific surface area per unit mass of particles (S_S) (Length^2. Mass^{-1}):

$$S_S = (\frac{6}{\rho_S})\sum\left(\frac{P_{NoD} - P_{Nod}}{d}\right) \tag{5}$$

where ρ_s is the density of soil particles, d is the smaller sieve size, P_{NoD}-P_{Nod} is the percentage by weight of particles between the larger sieve size D and smaller sieve size d, for particles smaller than the smallest physical sieve size, an equivalent diameter d_{eq} is needed for use in Eq. (5), given by (following Chapuis & Légaré [58]):

$$d_{eq} = \sqrt{\frac{{D_{min}}^2}{3}} \tag{6}$$

where D_{min} is the minimal measurable particle size. The specific surface area per volume (S_A) of the soil particles in this research is calculated as follows:

$$S_A = 6\sum\left(\frac{P_{NoD} - P_{Nod}}{d}\right) \tag{7}$$

with a similar derivation as Eq. (5) and with use of d_{eq} as required.

Ren & Santamarina [56] investigated the trend between k and e for wide range of sediments and provided:

$$\frac{k}{cm/s} = 10^{-5}\left(\frac{S_s}{m^2/g}\right)^{-2} e^{x} \tag{8}$$

where S_S is the specific surface area per unit mass of particles (Length^2. Mass^{-1}), the exponent x is obtained from a fitted power relation between k and e data available for each specific soil type and falls generally between 2 and 6. S_S of coarse grained soil can be estimated from the knowledge of particle size distribution and specific gravity (G_S) [56,58].

Study scope & aims

For this study, a granular soil database (CG/KSAT/7/1278, naming convention follows Phoon *et al.* [59]) of K test data and other infiltration related parameters was compiled. The hydraulic radius-based K prediction model (Eq.4) was calibrated and examined using this database. Eq. (4) is similar to the model from Ren & Santamarina [56] however in this work only a single exponent was used to characterise a wide range of soils rather than a range of exponents for each individual soil or test series. Ren & Santamarina [56] calibrated their model for a wider range of soil types with the vast majority being classified as 'clayey soils'. Feng & Vardanega [26,27] showed, using FG/KSAT-1358, the water content ratio (w/w_L) is an alternative predictor for the saturated coefficient of permeability. Therefore either the R_H or the w/w_L are valid predictors for saturated coefficient of permeability of fine-grained soil [26,27,56]. This paper focuses on developing a transformation model for a-priori estimation of the permeability of coarse-grained soils.

This paper aims to test the validity of a modified version of Ren & Santamarina's model [56] with a larger database of tests on granular soils and hypothesises that a single exponent can be fitted to the void ratio term which will result in a suitable transformation model for a-priori predictions of permeability of coarse-grained soils. The influence of the pore shape function $f(s)$ is not captured by this simplified model.

The aim of this work is to produce a calibrated transformation model that requires only knowledge of void ratio and material gradation and therefore the number of model parameters is minimised. The use of S_A as a predictor instead of S_S (as used in Ren & Santamarina [56]) also reduces the impact of unreported G_S on the developed model and keeps the model dimensionally consistent. The CG/KSAT/7/1278 database is also used to determine if Eq. (4) is statistically the best function for a-priori predictions of K. The effect of the soil fabric and the saturation level are out of scope for the present paper. This paper aims to study the K-related macroscopic characteristics and their effects upon the saturated K by using a compiled granular soil database (CG/KSAT/7/1278) (for further details on the database development and analysis see the recent doctoral thesis of Feng [60]).

DATABASE: CG/KSAT/7/1278

CG/KSAT/7/1278 consists of more than 1200 saturated K test data points on granular soils sourced from more than 50 publications. The database is expanded from an early version of the database which has only 164 datapoints (n)[1] ($n = 164$) and is presented in Feng *et al.* [61]. Information of the database includes the test method and test conditions. Some basic statistical measures of the studied parameters are summarised by the data sources in Table 2 together with their range of variation. Sources G2, G11, G25 and G29 (see Table 2) were also included in the database presented in Ren & Santamarina [56]. Both the saturation level and the hydraulic anisotropy are beyond the scope of this study, therefore, only saturated K data with water as permeant, measured vertically on granular soil with more than 50% of its grain particles larger than 0.75 mm were included in this database. Corey [114] reported that different level of saturation may lead to a range of K test result, for undisturbed sandy soil, the measured K ranges from 10% ($S_r = 70\%$) to 75% ($S_r = 96\%$) of its fully saturated K value.

The saturation process has been detailed or can be inferred based on the quoted test standard in most data sources. For cases without the saturation condition stated, given that the conventional K test methods usually include saturation process, it was assumed the k test was conducted under fully saturated conditions. All the k values were converted and presented as intrinsic K values based on the test temperature reported. 20 °C is assumed to be the default test temperature for the data sources where it is not quoted ($n = 200$). The quoted values of G_S in the database vary from 2.32 to 3.71. The average value of 2.69 ($n = 516$) was used for data entries without a reported value of G_s. (For the preferred transformation model adopted later in the paper G_s was not used directly in the calculation, however some of the database sources did state that the quoted e values were computed using an assumed G_s value (for instance G12 [73], G27 [88]).) The influence of including the datasets where G_s was not available, and where temperature was not directly stated is studied later in the paper.

Methodology: Statistical analysis

Model adequacy and outlier identification

The fitted regression models rely on certain assumptions, including residual normality, homoscedasticity, and independence. Violation of the regression assumptions may lead to inaccurate inferences in modelling [113–117] thus, analysis should be conducted to examine the fitting assumptions before interpreting any result. Pearson's correlation analysis is performed beforehand to assess the independence between predictors adopted in the fitted models. The normality of the residuals is assessed graphically by comparing the distribution of the residual against the expected normal distribution in quantile–quantile (Q-Q) plots. Normally distributed residuals tend to be linearly scattered in the Q-Q plot. The homoscedasticity is examined by checking the pattern of the residual versus predicted value plot. The residuals produced by the fitted model should be evenly distributed along the predicted (fitted) values in ideal situation, (see Montgomery *et al.* [117] p.303) for detailed demonstration on pattern checking).

To evaluate the effect of the outliers on the fitted model, regression analysis is again performed on a database with the identified outliers (large residuals and high leverage points) from the fitted model removed. Any observed datapoint with a standardized residual falling out of the −2 to 2 intervals [117] (p.303) or with a high leverage value which is more than 3 times of the mean leverage value (number of coefficients include intercept/ number of observations, Velleman & Welsch [118]) was defined as an outlier in this study.

Observations that appear as an outlier in at least 8 out of 11 of the fitted regression models were classified as a 'global outlier', which might not be 'typical' of the rest of the data. Regression analysis and model adequacy evaluations were then performed on the clean database with all 'global outliers' removed from the raw database. The processes of the outlier identification and the model adequacy evaluation are illustrated in Fig. 1. The complete analysis results from the outlier identification and model adequacy evaluation for all the models examined are presented in the online supplementary material (Figures S1-S35). The procedure for identifying statistical outliers used in this paper was used in Feng [60] and a similar approach was also used in Feng et al. [35].

Analysis

Regression analysis

The calibrated equations of all the examined prediction models using the database CG/KSAT/7/1278 are shown in Table 3. The initial regression analysis shows that the calibrated 'hydraulic radius' model (based on Eq.4 with a variable exponent on S_A) gives the most percentage of points falls within 0.1 to 10 times range (84.59%) with relatively evenly distributed predictions (56.34% overpredicted, 43.66% underpredicted), while the calibrated 'Taylor' equation yields the highest coefficient of determination (R^2) of 0.80. The predictions based on the calibrated 'Kozeny-Carman' equation are significantly skewed (see Figure S5 in the supplemental data), this is possibly due to some points with high leverage.

The model adequacy analysis includes the quantile–quantile plot for residual normality checking for the calibrated prediction models and the residual versus fitted value plot for homoscedasticity examination are summarised in online supplementary material (see Figures S1 to S11). The quantile–quantile plots show that the residuals from the calibrated linear-correlating models including the 'Hazen', 'Taylor' and 'Kozeny-Carman' appear less normally distributed compared to the other models being examined. The residual versus predicted value plots of the calibrated linear-correlating models ('Hazen', 'Taylor', 'Kozeny-Carman') all exhibit a 'funnel' pattern which represents anomalies and implies that a data transformation in the model may be required to eliminate the problem [117] (p.303). The outlier identification analysis showed notable changes in the regressed Kozeny-Carman coefficient after the elimination of the identified outliers (from 0.0008696 to 0.008085), while the variation in the regression coefficients and exponents of the other studied models is rather modest. After the elimination of the identified outliers, the prediction accuracy of the studied models is mostly enhanced with an increase in R^2 and a decrease in SE (see Table 3), while for the calibrated 'Taylor' model and 'Hazen' model, a reduction in both R^2 and SE are observed.

Hydraulic radius model adjustment

Examination of hydraulic radius fits in Table 3 shows the adjustment on the exponent of S_A is close to 2 (i.e. 1.785 to 1.860). The fitted

[1] The number of datapoints in a sample set (or subset) is denoted as n in this paper.

Table 2
Summary of the CG/KSAT/7/1278 database.

Source ID	Reference	Materials	n	K (mm^2) range	k test method	Permeant Test Temperature	e	D_{10}	D_{50}	G_S	C_U	C_Z
G01	Mavis & Wilsey [62]	Iowa river sand	12	5.66×10^{-5}-3.75×10^{-3}	CH	60°F	0.497–0.73	0.224–1.81	0.386–2.97	2.63	1.73–5.54	0.903–1.24
G02	Chu *et al.* [63]	Iowa sand	14	5.06×10^{-7}-9.33×10^{-5}	FH: rigid wall permeameter	corrected to 68°F	0.385–0.724	0.027–0.25	0.205–0.447	2.65–2.68	2–11.9	0.99–5.04
G03	Dudgeon [64]	Blue metal dolerite; Nepean sand; River gravel	6	1.48×10^{-4}-1.23×10^{-1}	CH	–	0.631–0.912	0.248–10.8	0.561–14.7	–	1.44–3.21	0.908–1.63
G04	Morris & Johnson [65]	Water-laid gravel; water-laid sand	7	8.56×10^{-7}-2.63×10^{-3}	CH for high or medium K, variable head for low K	60°F	0.395–0.805	0.00172–5.45	0.0771–8.64	2.61–2.71	1.56–47.2	0.986–31.5
G05	Bo [66][(a)]	Granite	7	2.96×10^{-4}-4.69×10^{-4}	CH	corrected to K	0.584–0.646	0.828	1.16	–	1.49	0.892
G06	Goetz [67]	Ottawa sand; Concrete sand; Dune sand; 22A gravel	19	9.36×10^{-6}-4.61×10^{-4}	CH (ASTM D2434)	23 °C	0.245–0.772	0.129–0.609	0.228–2.33	2.6–2.66	1.2–31.2	0.764–1.26
G07	Moulton & Seals [68]	Crushed limestone; Sand	9	3.17×10^{-6}-2.59×10^{-3}	CH	–	0.401–0.835	0.0952–1.14	0.208–10.9	2.65–2.72	1.82–32.3	1.2–3.02
G08	Shahabi *et al.* [69]	Natural sand	34	4.34×10^{-5}-2.77×10^{-4}	CH	corrected to 20 °C	0.475–0.625	0.284–0.315	0.387–1.74	–	1.49–6.67	0.798–2.52
G09	Highlands & Hoffman [70]	Subbase material	3	4.41×10^{-7}-7.76×10^{-3}	Fabricated FH, Standard constant permeameter	–	0.299–0.587	0.174–6.67	8.75–15.3	2.61	2.54–65.9	1.17–3.76
G10	Rockhold *et al.* [71]	Natural sand	1	9.21×10^{-6}	Guelph permeameter (CH)	–	0.639	0.225	0.616	–	3.16	1.06
G11	Chapuis *et al.* [72]	Sand	12	7.00×10^{-6}-3.00×10^{-5}	CH (ASTM D2434-68)	–	0.382–0.578	0.139	0.435	–	3.78	1.19
G12	Yeh & Harvey [73]	Sand	2	9.11×10^{-5}-1.13×10^{-4}	Steady-state infiltration experiment	–	0.754–0.832	0.284–0.475	0.415–0.735	–	1.62–1.66	0.951–1.01
G13	Olanrewaju & Wong [74]	Natural soil	2	4.01×10^{-5}-1.51×10^{-4}	CH	–	0.515–0.681	0.113–0.133	0.219–0.954	–	2.07–9.68	1.34–1.41
G14	Tangpithakkul [75]	Dense graded aggregate base material	5	2.56×10^{-6}-1.36×10^{-5}	CH (ASTM D2434)	corrected to 20 °C	0.383–0.79	0.479	5.25	2.65	15.5	1.12
G15	Heindel & Noyes [76]*	Subbase material	8	1.59×10^{-6}-8.58×10^{-4}	Vertical Lysimeter Testing, water head difference held constant	–	0.0939–0.257	0.112–0.753	0.459–14.1	–	5.09–75.3	1.04–7.83
G16	Hatanaka *et al.* [77]	Undisturbed sand sample	12	1.50×10^{-6}-4.18×10^{-5}	CH	–	0.8–1.1	0.00208–0.215	0.138–0.611	2.63–2.78	1.74–162	0.99–13.4
G17	Yin & Hachiya [78]	Single-sized crushed stone; Sand; Mechanical stabilized crushed stone	9	1.94×10^{-6}-3.36×10^{-2}	CH	–	0.233–0.565	0.144–11	0.288–14.9	2.45	1.42–36.5	0.89–1.63
G18	Tanaka *et al.* [79]	Toyoura sand; Lake Biwa sand	2	3.10×10^{-5}-8.64×10^{-5}	CH	15 °C	0.804–0.939	0.154–0.209	0.196–0.277	2.65–2.68	1.31–1.4	0.999–1.05
G19	Hatanaka *et al.* [80][(b)]	Sand	5	1.81×10^{-5}-5.06×10^{-5}	CH	13 °C to 18 °C	0.22–0.88	0.203–3.14	0.639–7.59	–	2.85–17.8	0.453–3.53
G20	Yang *et al.* [81]	Gravelly sand; Medium sand; Fine sand	3	2.05×10^{-5}-7.79×10^{-3}	CH (ASTM D2434)	–	0.538–0.699	0.157–2.72	0.308–4.83	2.6–2.65	1.9–4.3	0.905–0.99
G21	Rankine [82][(c)]	Hydraulic fills (sandy silts; silty sand and clay fraction)	14	5.97×10^{-8}-1.53×10^{-6}	CH, FH	–	0.58–0.72	0.00917–0.0351	0.0798–0.359	2.79–3.71	6.93–14.7	0.317–2.05
G22	Watabe & Saitoh [83][(d)]	Nagoya clay and Niigata sand mixture	15	5.84×10^{-12}-8.34×10^{-10}	Oedometer test	–	0.458–0.757	0.00702–0.00702	0.128–0.476	2.68	88.6	9.87
G23	Indrawan *et al.* [84]	Residual soil, Gravelly sand, medium sand mixture	9	9.96×10^{-9}-8.22×10^{-3}	CH (ASTM D2434)	–	0.47–0.762	0.00466–2.87	0.375–4.66	2.59–2.66	1.96–401	0.873–33

(*continued on next page*)

Table 2 (*continued*)

Source ID	Reference	Materials	*n*	*K* (mm^2) range	*k* test method	Permeant Test Temperature	*e*	D_{10}	D_{50}	G_S	C_U	C_Z
G24	Zhou *et al.* [10]	Sand and gravel mixture	9	6.14×10^{-5}-1.90×10^{-3}	CH	corrected to 20 °C	0.874–1.1	0.257–0.948	3.48–8.01	2.78	10.2–17.3	1.57–2.44
G25	Bandini & Sathiskumar [85]	Sand silts mixture	188	1.13×10^{-8}-2.33×10^{-6}	Triaxial cell (ASTM D5084)	corrected to 20 °C	0.337–0.669	0.0149–0.249	0.292–0.554	–	1.75–27.7	0.889–7.4
G26	Khoury *et al.* [86], Ghabchi *et al.* [87]	Anchor stone; Dolese aggregate; Martin Marietta aggregate	62	3.61×10^{-10}-7.01×10^{-4}	FH	corrected to 20 °C	0.13–0.61	0.0599–7.57	1.9–24.1	2.68–2.7	2.09–77.5	0.428–6.22
G27	Bouteldja *et al.* [88]	Alluvial sand; Alluvial gravel	12	6.65×10^{-5}-2.87×10^{-4}	Darcy permeameter (NF X30-441PR) (equivalent to ASTM D2434)	–	0.53–0.68	0.195–0.722	0.885–2.27	–	3.15–7.41	0.787–1.33
G28	Santillan & Campo [89]*	Rockfill dam material	2	7.13×10^{-7}-4.11×10^{-6}	Matsuo-Akai tests	–	0.199–0.237	0.102–0.308	5.8–9.96	2.61–2.76	59.4–108	0.81–1.39
G29	Indraratna *et al.* [90]	River sand	6	6.23×10^{-5}-1.40×10^{-4}	CH (ASTM D2434)	–	0.605–0.713	0.3	0.416–0.957	2.6–2.61	1.51–4.03	0.774–0.942
G30	Ören & Özdamar [5][(e)]	Natural zeolites	21	1.13×10^{-10}-8.60×10^{-6}	Rigid wall permeameter (ASTM D5856) (FH & CH)	–	0.966–1.47	0.255–0.385	0.159–1.09	–	1.98–4.61	1.23–2.91
G31	Dolzyk & Chmielewska [91]	Natural soil; subbase soil	24	1.07×10^{-6}-1.20×10^{-4}	CH	corrected to 10 °C	0.3–0.923	0.0713–0.336	0.169–12.1	–	1.95–60.8	0.181–1.87
G32	Chen *et al.* [92]	Natural clayey sand and cracked granite gravel mixture	8	7.25×10^{-6}-1.41×10^{-2}	CH	corrected to 20 °C	0.235–0.449	0.027–0.321	0.513–7.99	2.55–2.91	23.6–88	0.178–7.44
G33	Cetin *et al.* [93]	Unbound granular base materials	8	1.43×10^{-7}-2.76×10^{-5}	CH: rigid wall permeameter (ASTM D2434)	–	0.111–0.277	0.109–0.155	3.04–6.95	2.81–3.04	50.2–87.2	0.321–3.03
G34	Rosas *et al.* [94][(f)]	River sand; Offshore sand; Offshore sands-shallow marine mixed siliciclastic and carbonates; Dune sands; Beach sands	431	1.23×10^{-8}-9.89×10^{-6}	CH	corrected to 25 °C	0.235–0.938	0.0535–0.832	0.0827–3.13	–	1.31–18.3	0.532–2.57
G35	Jaafar & Likos [95]	Sand	1	1.54×10^{-5}	–	–	0.695	0.16	0.2	–	1.32	0.932
G36	Cai *et al.* [96][(g)]	Sandy sediments	14	5.13×10^{-7}-1.61×10^{-5}	CH	–	0.266–0.507	0.06–0.173	0.0975–0.332	2.65	1.7–2.81	0.876–1.22
G37	Liu [97]	Ottawa sand	45	6.97×10^{-7}-3.99×10^{-5}	CH (ASTM D2434); FH in triaxial apparatus	corrected to 20 °C	0.474–0.648	0.229	0.382	2.65	1.8	1.13
G38	Qiu & Wang [98]	Sandstone-Mudstone mixture	19	3.93×10^{-6}-5.72×10^{-5}	CH	corrected to 20 °C	0.377–0.534	0.178	3.05	2.68–2.71	26.4	1.03
G39	Nemes *et al.* [99]	Sand	4	4.09×10^{-6}-5.53×10^{-5}	–	–	0.429–0.786	0.109–0.263	0.165–0.356	–	1.44–2.49	0.906–1.12
G40	Cabalar & Akbulut [100]	Narli sand; Crushed stone sand	32	1.02×10^{-5}-2.51×10^{-3}	CH	20 ± 2 °C	0.52–1.02	0.0977–2.29	0.188–3.39	2.65–2.68	1.2–4.22	0.701–1.4
G41	Yang *et al.* [11]	River sand	9	9.64×10^{-7}-3.26×10^{-5}	CH	corrected to 20 °C	0.525–0.572	0.116–0.709	0.453–1.92	2.672	3.28–11.8	0.659–1.67
G42	Wang *et al.* [101]	Calcareous soil	20	1.01×10^{-7}-2.43×10^{-6}	CH	corrected to 20 °C	0.725–1.13	0.0252–0.143	0.214–0.448	2.78–2.8	3.3–10	1.07–3.21
G43	Feng [102]	Crushed basalt and gritstone mixure	30	4.29×10^{-4}-5.74×10^{-2}	CH (BSI 1377–5:1990)	corrected to 20 °C	0.535–0.852	0.721–5.82	2.2–10.5	2.72	1.93–6.94	0.696–3.21
G44	Mneina *et al.* [103]	Dense graded unbound granular material	8	1.23×10^{-10}-2.17×10^{-7}	CH: rigid-wall, compaction-mould permeameter (ASTM D5856)	corrected to 20 °C	0.111–0.29	0.06–0.604	2.82–8.74	–	12.8–77.9	0.834–3.69

(*continued on next page*)

Table 2 (*continued*)

Source ID	Reference	Materials	n	K (mm^2) range	k test method	Permeant Test Temperature	e	D_{10}	D_{50}	G_S	C_U	C_Z
G45	Chung *et al.* [104]	Joomunjin standard sand, Kaolinite, Gwanak granite soil, Songdo silty Clay mixture	14	1.00×10^{-10}-2.32×10^{-7}	Variable head test	–	0.238–0.754	0.000455–0.375	0.249–1.71	2.63–2.66	1.69–1270	0.382–615
G46	Bag *et al.* [105]	Bentonite; Sand	4	3.99×10^{-11}-7.26×10^{-7}	FH (flexible wall method)	–	0.495–0.675	0.00048–0.0735	0.33–0.537	2.67–2.68	8.11–1180	3.66–298
G47	Boley *et al.* [106]	Sand; Gravel	3	1.55×10^{-5}-3.05×10^{-4}	–	–	0.563–0.667	0.16–1.9	0.303–3.53	–	2.09–2.57	0.962–1.16
G48	Gao *et al.* [107]; Dong *et al.* [108]	Eluvial-colluvial gravelly soil	5	1.19×10^{-8}-1.88×10^{-5}	CH	–	0.238–0.406	0.138–0.256	0.897–5.04	2.32	9.97–34	0.732–1.73
G49	Shamsuddin *et al.* [109](*)	Riverbank sediment	5	4.36×10^{-8}-8.11×10^{-7}	In situ FH	28 °C	0.389–0.667	0.105–0.654	0.624–1.86	–	4.13–14.2	0.536–1.43
G50	Taiba *et al.* [110]	Chlef sand, Hostun sand, Fontainebleau sand, Silt mixtures	12	9.24×10^{-7}-2.24×10^{-5}	CH	20 °C	0.644–0.954	0.00963–0.26	0.174–0.577	2.64–2.66	1.58–53.9	0.961–8.46
G51	Arshad *et al.* [111]	Sand mixture	17	9.31×10^{-7}-3.58×10^{-4}	CH (AASHTO T215)	20 °C	0.32–0.6	0.013–0.482	0.107–0.783	2.44–2.72	1.79–48.5	0.0939–17.9
G52	Rees *et al.* [112]	Conglomerate	1	1.13×10^{-3}	FH	–	0.492	0.29	1.43	–	8.25	0.687
G53	Toumpanou *et al.* [113]	Sand-sized crushed limestone	54	3.07×10^{-6}-3.33×10^{-3}	CH (ASTM D2434)	Corrected to 20 °C	0.42–0.76	0.08–2.15	0.108–2.92	2.71	1.23–15.8	0.55–3.74

Notes: CH = Constant head test; FH = Falling head test; (*) data from field testing; (a) readings recorded within the first 8hrs of testing are averaged; (b) Part of the gradation data is not recognizable; (c) k values in the sources are averaged from the results of the CH and FH testing; (d) gradation information given as volumetric percentage; (e) void ratio calculated based on reported dry density and specific gravity; (f) void ratio calculated based on calibrated model in the original source; (g) porosity measured by tracer.

hydraulic radius model was adjusted to conform the theoretical requirement of 2, the adjusted model to a fixed exponent on S_A of 2 using CG/KSAT/7/1278 gives:

$$K = 1.78 \times 10^{-2} e^{2.459} / {S_A}^2 \tag{9}$$

Eq. (9) gives 84.51% of the predictions within 0.1 to 10 times of the measured K, with 53.29% over prediction and 46.71% under prediction, which generally gives same level of prediction strength as the fitted hydraulic radius model with variable exponent (84.59% within 0.1 to 10 times range, 56.34% overpredicted and 43.66% underpredicted). Fig. 2 compares the predicted and measured K values from CG/KSAT/7/1278 using both models and shows that the adjusted hydraulic radius model with a fixed exponent on S_A of 2 gives sufficiently close predictions compared to the variable exponent model over the entire database CG/KSAT/7/1278. Fig. 2 is presented as a measured versus predicted plot (see Piñeiro *et al.* [119]).

Regression analysis (with outliers removed)

The outlier identification analysis of the full database reveals that some high leverage and/or large standardized residual points could be substantially influential to the calibrated outcome of the examined prediction models. To mitigate the influence from the outliers, and to avoid unduly discarding the contradictory information of the examined model, only observations identified as outliers in at least 8 out of the 11 fitted models were classified as 'global outliers' and hence removed from the studied database. In total, 22 out of 1278 (1.72%) datapoints were removed, regression analysis results based on the database with the identified global outliers removed are shown in Table 4. Eq. (6) is of a nonlinear form, for which R^2 would be an inadequate statistical measure [120] and hence R^2 was not used in the following model comparison analysis. Instead the following regression models were judged according to the following criteria: (i) the percentage of the data predicted by the transformation model falling within $y = 0.1x$ and $y = 10x$; (ii) skewness of the predictions from the new transformation model i.e. a comparison of the percentage of points over or underpredicted by the model and (iii) that ideally the model would be dimensionless.

Among all the models trialled, the 'water content ratio' model (Feng & Vardanega [26,27]: note e/S_S as an equivalent substitute of w/w_L for granular soil) provides most predictions within the 0.1 to 10 times bound (85.35%), albeit marginal improvement over the 'hydraulic radius' model (85.19%), while the predictions from the 'hydraulic radius' model are less biased. Statistically reliable predictions can be achieved by using the effective particle size D_{10} (i.e., the 'Shepherd' model) which often is an indicator of pore sizes [1,36,37], the inclusion of the e parameter may enhance the accuracy, however the improvement is modest (i.e. 'Chapuis' model). The prediction accuracy of the grading entropy models is improved with the inclusion of void ratio as suggested by O'Kelly & Nogal [12] (see also Feng *et al.* [34]), still the correlation is not as strong as the models based on other predictors for K.

The model adequacy analysis (see Figures S12 to S22 in the supplementary data) shows that compared to the other models, the residual distribution of the linear calibrated linear-correlating models ('Hazen', 'Taylor', 'Kozeny-Carman') diverges more from the normal distribution, while the residual versus predicted value plots for the linear-correlating models ('Hazen', 'Taylor', 'Kozeny-Carman') again exhibit an anomaly 'funnel' pattern suggesting possible need for data transformation.

Results from the regression analysis and model adequacy examination based on both the full and the cleaned database (Tables 3 and 4) show that the 'hydraulic radius' model and the 'water content ratio' model (see Figs. 3 to 6) overall give the most accurate estimation of the K for the assembled granular database CG/KSAT/7/1278 in terms of prediction accuracy (percentage of prediction within $0.1x$ to $10x$ bounds) and prediction skewness (over/ under prediction). The 'hydraulic radius' model is dimensionally homogeneous, has high statistical

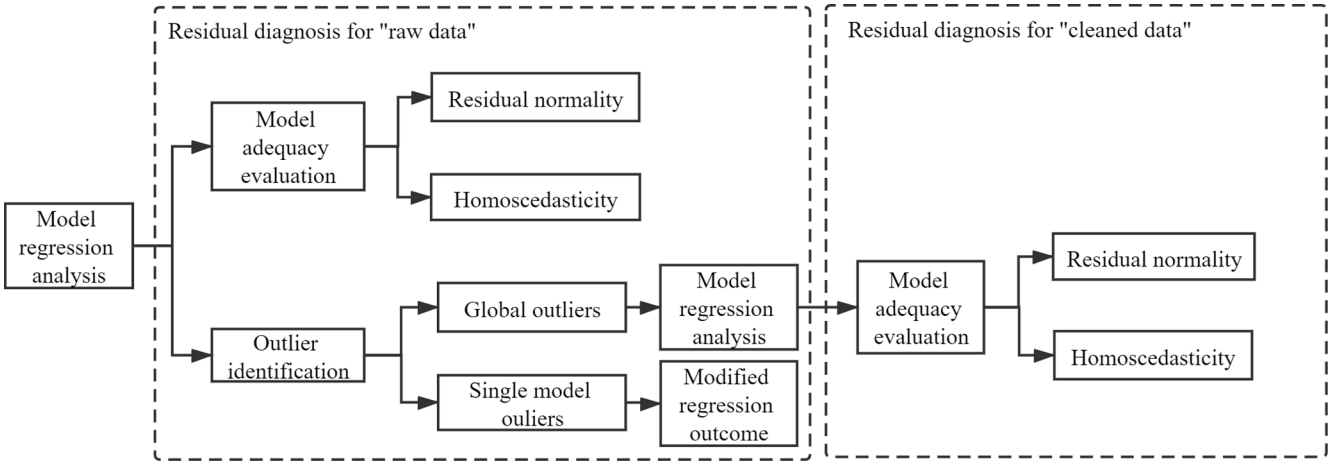

Fig. 1. Process for model adequacy evaluation.

reliability (and model adequacy) and is thus favoured among all the K prediction models examined using this database.

The constants (α and β) from Eq. (4) have been calibrated using a new database. Global outliers have been removed using the procedure outlined in this paper. The calibrated transformation model is:

$$K = 1.693 \times 10^{-2} \frac{e^{2.283}}{{S_A}^2} \quad (n = 1256)\ (\alpha = 1.693 \times 10^{-2} \text{ and } \beta = 2.283) \tag{10}$$

Eq. (10) is dimensionally homogeneous and does not require a varying exponent on the e term and has no appreciable loss of prediction accuracy compared to the other empirical models studied (Table 1). In the next section potential influences on the α and β values are studied including: (i) the assumption of some permeant testing temperature values, (ii) void ratio level, (iii) soil gradation, (iv) permeability testing type and (v) influence of individual data sources.

Analysis: Data subsets

Known testing temperature

Recalling that the assumption of a 20 °C test temperature was used to convert the k values from the original sources to K for 192 out of 1256 data points used to generate the calibrated equations. The effect of this assumption is studied in this section. Fig. 7 gives the measured versus predicted plot using the 'hydraulic radius' model using only the data sources from the cleaned database with a reported test temperature. The coefficient and exponent of the fitted model do vary to some extent (compare Fig. 6 and Fig. 7), and the prediction accuracy enhanced marginally from 85.19% (with the 20 °C assumption) to 89.29% (without the 20 °C assumption). Table 5 shows a numerical comparison of the two equations from Figs. 6 and 7 which shows that the equation from Fig. 7 yields increasingly higher predictions as e increases (however, the factor increase is not considerable when $e < 1$ especially when placed in the context of the accuracy of the K testing in general). Fig. 8 shows the spread of e-values across the database indicating that most of the data ranges from around 0.41 to 0.77 (i.e. approximately the mean plus or minus 1 standard deviation: Fig. 8). It is recognised that the 20 °C assumption for data sources without a reported test temperature does have some impact on the fitted model. However, the assumption of 20 °C test temperature was retained for the following study of various database subsets to maximise the data available in analysis.

Void ratio level

To examine potential variation of the exponent on the void ratio function, the database was subdivided based on the void ratio range. Given that void ratio greater than 1 are rare for soils [53], it was decided to investigate soils above this void ratio threshold and then subdivide the range 0 to 1 equally (which gives $n = 818$ (subset '$0.5 \le e < 1$') and $n = 409$ (subset '$e < 0.5$')) and investigate the effect on the fitted regressions of these subdivisions. The analysis result of the equations calibrated based on Eq. (4) for all data subsets are summarised in Table 6. The calibrated transformation model gives a statistically reliable prediction ($p < 0.0001$)[2] for all data subsets, while the '$0.5 \le e < 1$' subset yields the most predictions within the 0.1 to 10 times range (89.24%, $n = 818$). Minor variation of the calibrated equation can be seen across the subsets '$e < 0.5$', '$0.5 \le e < 1$' and '$e < 1$'(coefficient ranges from 2.098×10^{-2} to 2.959×10^{-2}, exponent ranges from 2.585 to 3.437). There is a considerable reduction in the exponent of the calibrated equation for the data subset '$e \ge 1$' comparing to all the subsets with a void ratio level less than 1 (from around 3 to −13): the relatively small sample size of this subset should be noted. For further information on the best fit distributions for the key parameters of CG/KSAT/7/1278 see (Feng [60] and Feng *et al.* [121]).

Gradation parameters

Informed by the unified soil classification system [122], the database was classified into 'sand ($D_{50} < 4.75$ mm)', 'gravel ($D_{50} > 4.75$ mm)', '$C_U \ge 6$', '$C_U < 6$', '$1 \le C_Z \le 3$' (the coefficient of curvature), '$1 > C_Z$ or $C_Z > 3$' subsets (noting that, 24 data points could not be categorized based on either C_U or C_Z due to the absence of D_{10} information). Table 7 presents analysis results for all the data subsets. Statistically strong correlations can be seen for all subsets and the calibrated exponent fluctuates from 1.911 to 3.624. Better prediction of K can be achieved in the 'sand' data subset than the 'gravel' data subset, while the regression equation based on '$C_U < 6$' subset gives the most accurate prediction among all the sub-datasets with more than 90% of the predicted value within the 0.1 to 10 times range and nearly equally distributed along the line of equality. By comparing the analysis result of '$C_U < 6$' subset to the whole database, it can be inferred that the prediction strength of Eq. (4) can be noticeably enhanced with the exclusion of soils with wide-ranging particle size distributions ($C_U \ge 6$) (from 75.99% to 90.48% within 0.1x to 10x bounds).

Test type

The database CG/KSAT/7/1278 consists of data from different K test

[2] p is the p-value of the regression equation.

Table 3
Summary of regression results based on the full database.

Model Type	*n*	Calibrated model	R^2	Standard Error *(SE)*	% between $y = 0.1x$ and $y = 10x$	% over-predicted	% under-predicted	Fig.	Remarks
Effective particle size									
Hazen [16–18]	1254	$K = 0.000325{D_{10}}^2$	0.32	0.0038	81.66%	67.22%	32.78%	S1	Data points without available D_{10} information are not included. Same for the below.
Adjusted model	1206	$K = 0.000286{D_{10}}^2$	0.24	0.00066	Points excluded*: 34 ESR; 44 LLP.				
Shepherd [19]	1254	$K = 1.042 \times 10^{-4}{D_{10}}^{1.731}$	0.54	2.04	79.82%	53.27%	46.73%	S2	Regression equation: $lnK = -9.169 + 1.731 lnD_{10}$
Adjusted model	1129	$K = 2.618 \times 10^{-4}{D_{10}}^{2.095}$	0.68	1.41	Points excluded*: 69 ESR; 68 LLP.				Adjusted regression equation: $lnK = -8.248 + 2.095 lnD_{10}$
Chapuis [20]	1254	$K = 6.037 \times 10^{-4}(\frac{{D_{10}}^2 e^3}{1+e})^{0.829}$	0.58	1.94	81.9%	56.78%	43.22%	S3	Regression equation: $lnK = -7.412 + 0.829 ln(\frac{{D_{10}}^2 e^3}{1+e})$
Adjusted model	1146	$K = 1.106 \times 10^{-3}(\frac{{D_{10}}^2 e^3}{1+e})^{0.917}$	0.69	1.42	Points excluded*: 66 ESR; 51 LLP.				Adjusted regression equation: $lnK = -6.807 + 0.917 ln(\frac{{D_{10}}^2 e^3}{1+e})$
Taylor [1]	1254	$K = 0.003089\frac{{D_{10}}^2 e^3}{1+e}$	0.80	0.0021	80.46%	67.78%	32.22%	S4	
Adjusted model	1146	$K = 0.003503\frac{{D_{10}}^2 e^3}{1+e}$	0.44	0.00057	Points excluded*: 43 ESR; 23 LLP.				
Specific surface/ specific surface area per volume									
Kozeny [21], Carman [22,23]	1278	$K = 0.0008696\left(\frac{1}{{S_A}^2}\right)\left(\frac{e^3}{1+e}\right)$	0.33	0.0038	13.38%	4.225%	95.77%	S5	The original regression equation is largely biased due to some high leverage points (see Figure S5).
Adjusted model	1259	$K = 0.008085\left(\frac{1}{{S_A}^2}\right)\left(\frac{e^3}{1+e}\right)$	0.09	0.00063	Points excluded*: 19 ESR; 2 LLP.				
Feng & Vardanega [26,27]	1278	$K = 3.772 \times 10^{-9}(e/S_S)^{1.814}$	0.64	1.97	84.27%	55.16%	44.84%	S6	Regression equation: $lnK = -19.396 + 1.814\ln(e/S_S)$
Adjusted model	1160	$K = 2.716 \times 10^{-9}(e/S_S)^{1.918}$	0.74	1.33	Points excluded*: 84 ESR; 52 LLP.				Adjusted regression equation: $lnK = -19.724 + 1.918\ln(e/S_S)$
Hydraulic radius (variable exponent)	1278	$K = 8.14 \times 10^{-3}\frac{e^{2.407}}{{S_A}^{1.785}}$	0.64	1.96	84.59%	56.34%	43.66%	S7	Regression equation: $lnK = -4.811 + 2.407 lne - 1.785 lnS_A$
Adjusted model	1148	$K = 1.42 \times 10^{-2}\frac{e^{2.747}}{{S_A}^{1.860}}$	0.77	1.29	Points excluded*: 81 ESR; 60 LLP.				Adjusted regression equation: $lnK = -4.252 + 2.747 lne - 1.860 lnS_A$
Grading entropy									
Feng *et al.* [31] modified	1276	$K = 1.35 \times 10^{-40}{S_0}^{26.76}\Delta S^{-2.701}$	0.47	2.39	72.57%	46.16%	53.84%	S8	Regression equation: $lnK = -91.80 - 2.701 ln\Delta S + 26.76 lnS_0$
Adjusted model	1184	$K = 1.106 \times 10^{-43}{S_0}^{28.33}\Delta S^{-3.051}$	0.60	1.71	Points excluded*: 75 ESR; 28 LLP.				Adjusted regression equation: $lnK = -98.91 - 3.051 ln\Delta S + 28.33 lnS_0$
Feng *et al.* [34]	1276	$K = 9.822 \times 10^{-6}A^{-0.253}B^{-0.739}e^{1.788}$	0.049	3.20	60.34%	54.7%	45.3%	S9	Regression equation: $lnK = -11.531 - 0.253 lnA - 0.739 lnB + 1.788 lne$
Adjusted model	1170	$K = 1.931 \times 10^{-5}A^{0.985}B^{3.080}e^{2.051}$	0.085	2.35	Points excluded*:76 ESR; 33 LLP.				Adjusted regression equation: $lnK = -10.855 + 0.985 lnA + 3.080 lnB + 2.051 lne$
Feng *et al.* [34] modified	1276	$K = 1.276 \times 10^{-44}{S_0}^{30.27}\Delta S^{-1.989}e^{3.054}$	0.56	2.18	76.96%	49.61%	50.39%	S10	Regression equation: $lnK = -101.07 + 30.27 lnS_0 - 1.989 ln\Delta S + 3.054 lne$
Adjusted model	1178	$K = 1.453 \times 10^{-44}{S_0}^{30.489}\Delta S^{-2.710}e^{3.092}$	0.68	1.53	Points excluded*: 72 ESR; 38 LLP.				Adjusted regression equation: $lnK = -100.94 + 30.489 lnS_0 - 2.710 ln\Delta S + 3.092 lne$
Feng *et al.* [35]	1276	$K = 6.409 \times 10^{-38}S^{24.18}e^{4.027}$	0.33	2.69	67.24%	52.82%	47.18%	S11	Regression equation: $lnK = -85.64 + 24.18 lnS + 4.027 lne$
Adjusted model	1172	$K = 4.598 \times 10^{-37}S^{23.685}e^{4.237}$	0.44	2.01	Points excluded*: 64 ESR; 57 LLP.				Adjusted regression equation: $lnK = -83.67 + 23.685 lnS + 4.237 lne$

* ESR = extreme standardized residual; LLP = large leverage point; the extreme standardized residual and the large leverage point may overlap.

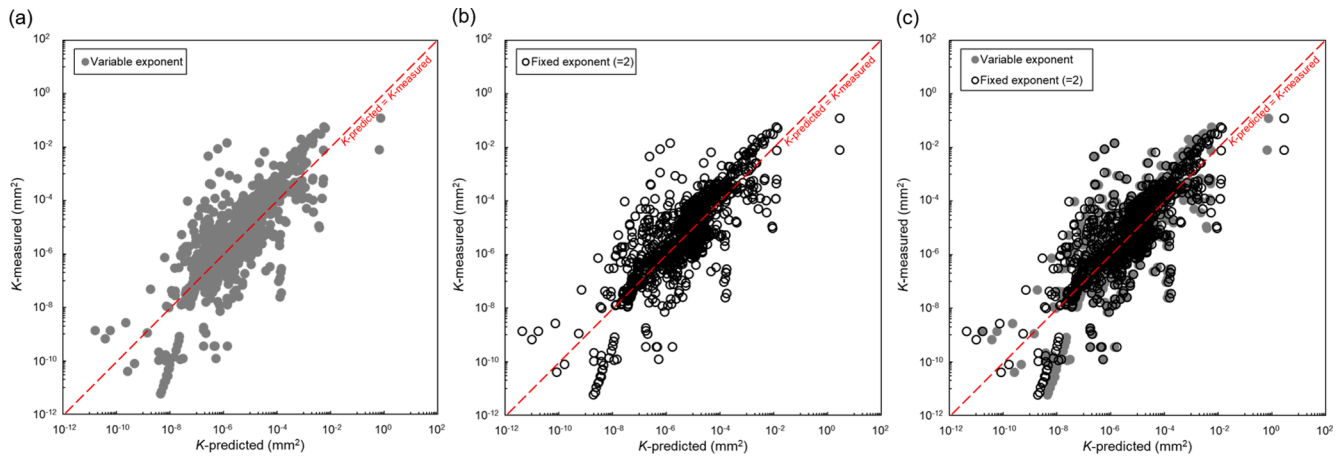

Fig. 2. Model comparison with variable exponent and fixed exponent on S_A.

Table 4
Summary of regression result based on the full database with outliers removed.

Model Type	*n*	Calibrated Model	% between $y = 0.1x$ and $y = 10x$	% over-predicted	% under-predicted	Fig.	Remarks
Hazen [16–18]	1232	$K = 0.0001519{D_{10}}^2$	82.06%	44.32%	55.68%	S12	Data points without available D_{10} information are not included. Same for the below.
Shepherd [19]	1232	$K = 1.071 \times 10^{-4}{D_{10}}^{1.712}$	81.09%	55.52%	44.48%	S13	Regression equation: $lnK = -9.142 + 1.712lnD_{10}$
Chapuis [20]	1232	$K = 5.786 \times 10^{-4}(\frac{{D_{10}}^2 e^3}{1+e})^{0.8146}$	83.36%	57.95%	42.05%	S14	Regression equation: $lnK = -7.455 + 0.8146\left(\frac{{D_{10}}^2 e^3}{1+e}\right)$
Taylor [1]	1232	$K = 0.002369\left(\frac{{D_{10}}^2 e^3}{1+e}\right)$	83.6%	61.61%	38.39%	S15	
Kozeny [21], Carman [22,23]	1256	$K = 0.05421\left(\frac{1}{{S_A}^2}\right)\left(\frac{e^3}{1+e}\right)$	83.76%	63.3%	36.7%	S16	
Feng & Vardanega [26,27]	1256	$K = 3.799 \times 10^{-9}(e/S_S)^{1.827}$	85.35%	57.32%	42.68%	S17	Regression equation: $lnK = -19.388 + 1.827ln(\frac{e}{S_S})$
Hydraulic radius (this study)*	1256	$K = 1.693 \times 10^{-2}\frac{e^{2.283}}{{S_A}^2}$	85.19%	54.38%	45.62%	S18	
Feng *et al.* [31] modified	1254	$K = 1.31 \times 10^{-41}{S_0}^{27.52}\Delta S^{-2.552}$	74.56%	49.12%	50.88%	S19	Regression equation: $lnK = -94.14 + 27.52lnS_0 - 2.552ln\Delta S$
Feng *et al.* [34]	1254	$K = 8.219 \times 10^{-6}A^{-0.2798}B^{-0.633}e^{1.493}$	62.2%	54.86%	45.14%	S20	Regression equation: $lnK = -11.71 - 0.2798lnA - 0.633lnB + 1.493lne$
Feng *et al.* [34] modified	1254	$K = 7.15 \times 10^{-45}{S_0}^{30.42}\Delta S^{-1.977}e^{2.734}$	78.47%	51.44%	48.56%	S21	Regression equation: $lnK = -101.60 + 30.42lnS_0 - 1.977ln\Delta S + 2.734lne$
Feng *et al.* [35]	1254	$K = 1.372 \times 10^{-37}S^{23.88}e^{3.654}$	68.66%	53.99%	46.01%	S22	Regression equation: $lnK = -84.88 + 23.88lnS + 3.654lne$

types. To examine the effect of the K test type, based on the adopted K test mechanism, the database was divided into 'constant head test', 'falling head test' and 'other test method' sub datasets. Table 8 summarises the analysis results for these three subsets. As can be seen from Table 8 some degree of variation does appear in the calibrated prediction models, while models in the form of Eq. (4) for all sub datasets have $p < 0.0001$.

Effect of individual data sources

Six individual data sources were selected to study the effect of their removal on the α and β values from Eq. 4 and 10. The datasets selected were G34 (largest individual data source); G25 (second largest individual data source); G26 (third largest individual data source); G53 (fourth largest individual data source); G22 (individual data source with lower K values) and G43 (individual data source with higher K values). Table 9 shows the effects on the α and β values from removal of each of these individual data-subsets (see also Figures S36 to S41) compared with two examples from the earlier analysis i.e. removal of test data points with assumed test temperature and restriction of the database to $0.5 \leq e < 1$. Table 9 shows that while removal of an individual data-source can change the α and β values by up to 20% (for the examples considered in this paper) the effect of restricting the data-set based on void ratio, gradation, test type can be shown to change the α and β values more in some cases (cf. Tables 6 to 8). The effects on the α and β values with the data sources removed where G_s was not specified are shown on Fig. S42 (i.e. $\alpha = 3.2285 \times 10^{-2}$ and $\beta = 2.542$).

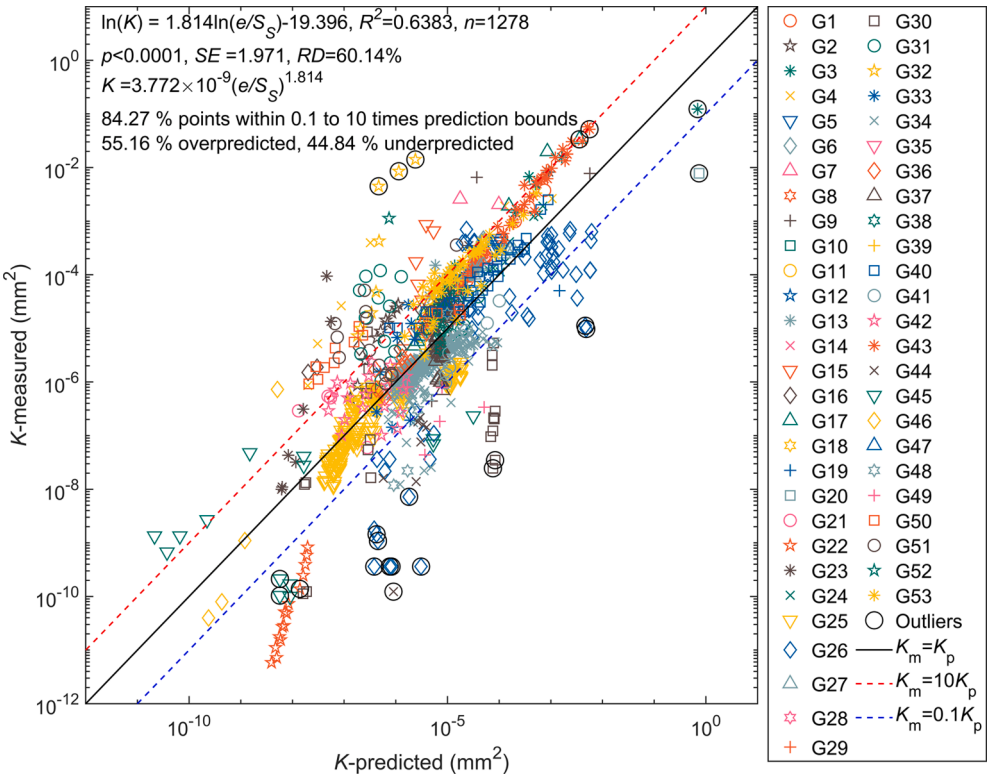

Fig. 3. *K*-measured (K_m) versus *K*-predicted (K_p) using 'water content ratio' model based on the full database (data source numbering follows Table 2).

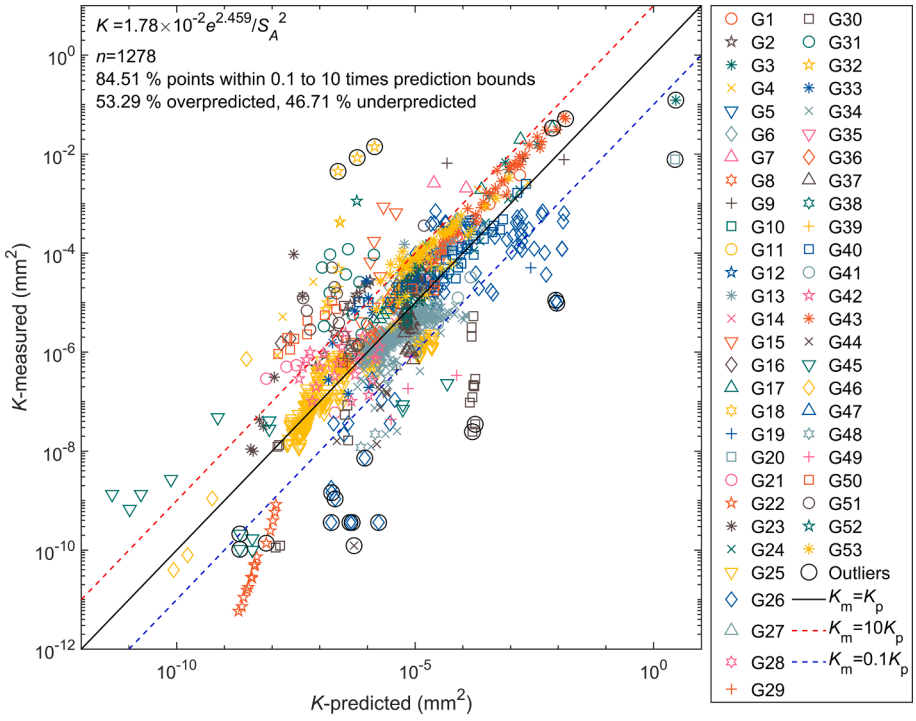

Fig. 4. *K*-measured (K_m) versus *K*-predicted (K_p) using 'hydraulic radius' model based on the full database (data source numbering follows Table 2).

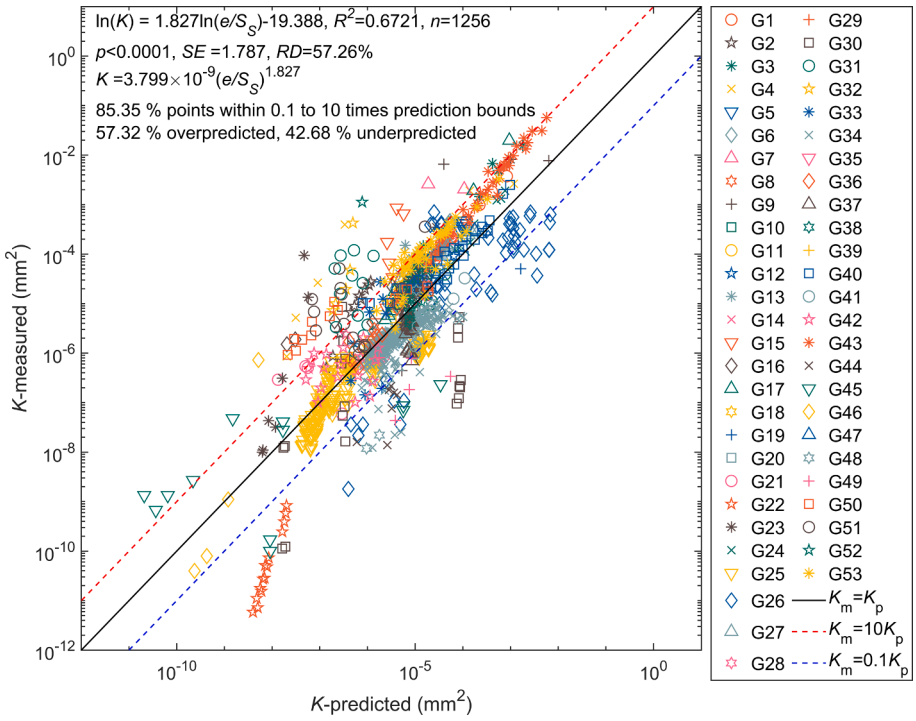

Fig. 5. *K*-measured (K_m) versus *K*-predicted (K_p) using 'water content ratio' model based on the cleaned database (data source numbering follows Table 2).

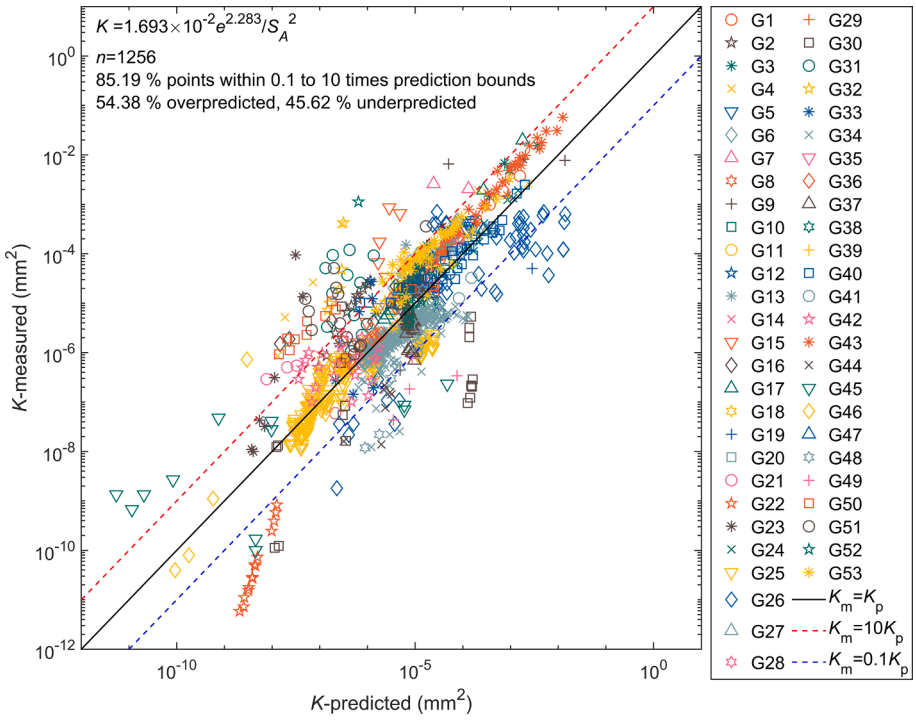

Fig. 6. *K*-measured (K_m) versus *K*-predicted (K_p) using 'hydraulic radius' model based on the cleaned database (data source numbering follows Table 2).

Summary & Conclusions

A new database (CG/KSAT/7/1278) has been assembled and contains over 1200 saturated *k* measurements on granular materials. The database has been used to calibrate various models for *K*. A transformation model for granular soil *K* (based on Eq.4) has been proposed and calibrated using the database with outliers removed based on a detailed statistical analysis:

$$K = 1.693 \times 10^{-2} \frac{e^{2.283}}{S_A{}^2} \tag{10bis}$$

Eq. (10) is dimensionally homogeneous and does not require a varying exponent on the *e* term and has no appreciable loss of prediction accuracy compared to the other empirical models studied (Table 1). Compared to the Ren & Santamarina [56] approach (Eq.8), the simplified hydraulic radius model (Eq.4) does not require the specific gravity

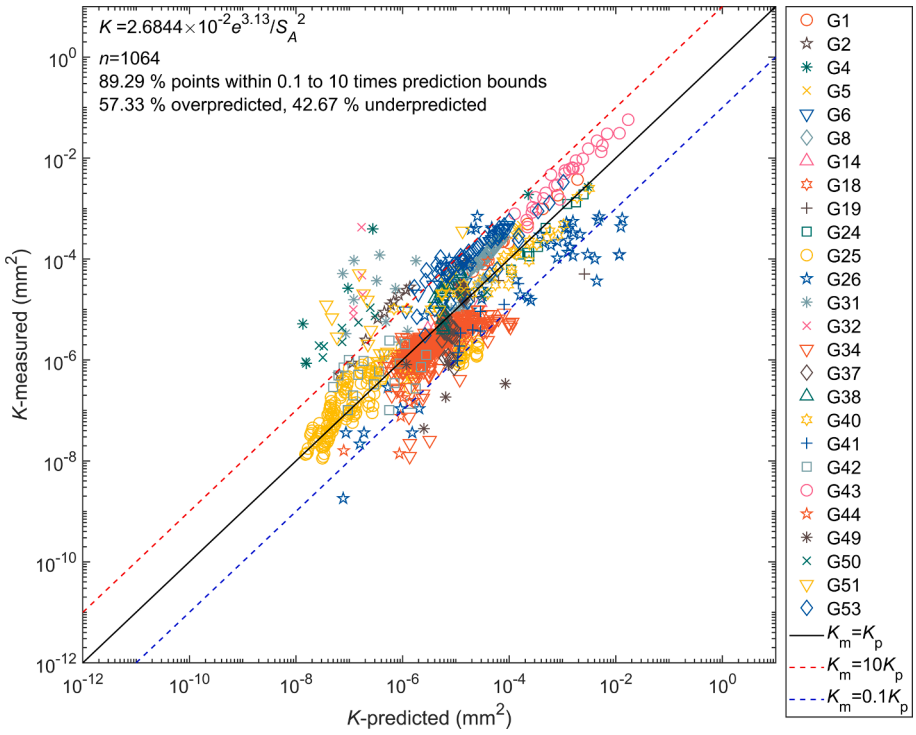

Fig. 7. *K*-measured (K_m) versus *K*-predicted (K_p) using 'hydraulic radius' model based on data sources from the cleaned database with a reported test temperature (data source numbering follows Table 2).

Table 5
Comparison of fitted equations from Figs. 6 and 7.

e	$K(S_A^2)$ – Fig. 6	$K(S_A^2)$ – Fig. 7	Approximate factor increase from Fig. 6 equation to the Fig. 7 equation
0.25	0.000715	0.00035	0.49
0.5	0.003479	0.003066	0.88
0.75	0.008779	0.01091	1.24
1.0	0.01693	0.02684	1.59
1.25	0.02818	0.05397	1.92

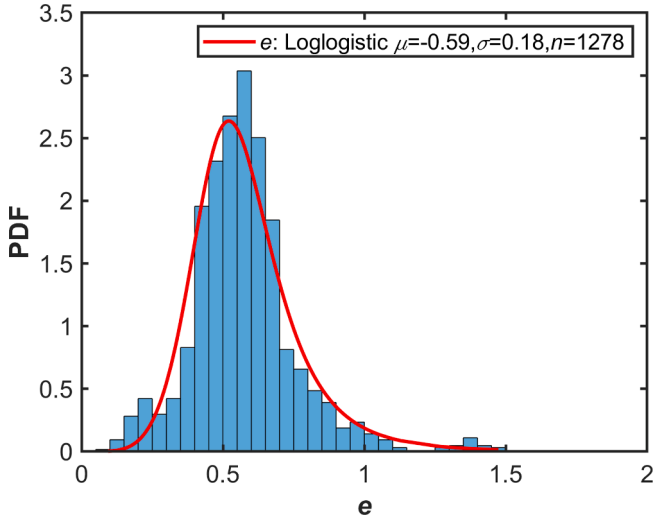

Fig. 8. Distribution of void ratio values from CG/KSAT/7/1278.

Table 6
Analysis results for data subsets divided by void ratio level (all regression results $p < 0.0001$).

Subset	*n*	Calibrated Model	% within 0.1x to 10x bounds	Figure
$e < 0.5$	409	$K = 2.610 \times 10^{-2} e^{2.698} {S_A}^{-2}$	78.97%	S23
$0.5 \le e < 1$	818	$K = 2.959 \times 10^{-2} e^{3.437} {S_A}^{-2}$	89.24%	S24
$e < 1$	1224	$K = 2.098 \times 10^{-2} e^{2.585} {S_A}^{-2}$	86.03%	S25
$e \ge 1$	32	$K = 8.024 \times 10^{-2} e^{-12.67} {S_A}^{-2}$	68.75%	S26

Table 7
Analysis results for data subsets divided by gradation parameter range (all regression results $p < 0.0001$).

Subset	*n*	Calibrated Model	% within 0.1x to 10x bounds	Figure
sand	1137	$K = 1.384 \times 10^{-2} e^{1.911} {S_A}^{-2}$	86.9%	S27
gravel	119	$K = 3.588 \times 10^{-2} e^{3.225} {S_A}^{-2}$	70.59%	S28
$C_U \ge 6$	329	$K = 9.028 \times 10^{-2} e^{3.624} {S_A}^{-2}$	75.99%	S29
$C_U < 6$	903	$K = 1.342 \times 10^{-2} e^{2.139} {S_A}^{-2}$	90.48%	S30
$1 \le C_Z \le 3$	565	$K = 1.607 \times 10^{-2} e^{2.065} {S_A}^{-2}$	84.25%	S31
$1 > C_Z$ or $C_Z > 3$	667	$K = 2.369 \times 10^{-2} e^{2.832} {S_A}^{-2}$	88.46%	S32

Table 8
Analysis results for data subsets divided by K test type (all regression results $p < 0.0001$).

Subset	n	Calibrated Model	% within 0.1x to 10x bounds	Figure
constant head test	923	$K = 1.806 \times 10^{-2} e^{2.113} {S_A}^{-2}$	89.49%	S33
falling head test	90	$K = 5.456 \times 10^{-2} e^{4.123} {S_A}^{-2}$	60%	S34
other test methods	243	$K = 1.984 \times 10^{-3} e^{-0.0837} {S_A}^{-2}$	89.3%	S35

Table 9
Effect of removal of individual data-sets on the calibration parameters of Eq. (4) (see Table 2 for the source numbering).

Data-set	Notes	Fig.	n	α	$\triangle\alpha$ (compared to Fig. 6)	β	$\triangle\beta$ (compared to Fig. 6)
G01-G53	Cleaned data-set ($n = 1256$) For G01-G53: $5.84 \times 10^{-12} \leq K\ (\mathrm{mm}^2) \leq 5.74 \times 10^{-2}$	6	1256	1.693×10^{-2}	–	2.283	–
G01-G53 excluding G34	Cleaned data-set ($n = 1256$) excluding the largest individual data source i.e. G34 ($n = 431$, pre-database cleaning) For G34: $1.23 \times 10^{-8} \leq K\ (\mathrm{mm}^2) \leq 9.89 \times 10^{-6}$	S36	825	2.7279×10^{-2}	1.0349×10^{-2} (61%)	2.466	0.183 (8.0%)
G01-G53 excluding G25	Cleaned data-set ($n = 1256$) excluding the second largest individual data source i.e. G25 ($n = 188$, pre-database cleaning) For G25: $1.13 \times 10^{-8} \leq K\ (\mathrm{mm}^2) \leq 2.33 \times 10^{-6}$	S37	1068	1.8502×10^{-2}	0.1572×10^{-2} (9.3%)	2.329	0.046 (2.0%)
G01-G53 excluding G26	Cleaned data-set ($n = 1256$) excluding the third largest individual data source i.e. G26 ($n = 62$ pre-database cleaning) For G26: $3.61 \times 10^{-10} \leq K\ (\mathrm{mm}^2) \leq 7.01 \times 10^{-4}$	S38	1203	1.4003×10^{-2}	-0.2927×10^{-2} (-17%)	1.835	−0.448 (-20%)
G01-G53 excluding G53	Cleaned data-set ($n = 1256$) excluding the fourth largest individual data source i.e. G53 ($n = 54$ pre-database cleaning) For G53: $3.07 \times 10^{-6} \leq K\ (\mathrm{mm}^2) \leq 3.33 \times 10^{-3}$	S39	1202	1.5446×10^{-2}	-0.1484×10^{-2} (-8.8%)	2.258	−0.025 (-1.1%)
G01-G53 excluding G22	Cleaned data-set ($n = 1256$) excluding an individual data source with low K values i.e. G22 ($n = 15$ pre-database cleaning) For G22: $5.84 \times 10^{-12} \leq K\ (\mathrm{mm}^2) \leq 8.34 \times 10^{-10}$	S40	1242	1.8142×10^{-2}	0.1212×10^{-2} (-7.2%)	2.313	0.03 (1.3%)
G01-G53 excluding G43	Cleaned data-set ($n = 1256$) excluding an individual data source with high K values i.e. G43 ($n = 30$ pre-database cleaning) For G43: $4.29 \times 10^{-4} \leq K\ (\mathrm{mm}^2) \leq 5.74 \times 10^{-2}$	S41	1227	1.5769×10^{-2}	-0.1161×10^{-2} (-6.9%)	2.222	−0.061 (-2.8%)
G01-G53*	Data-points with unknown test temperature excluded (inc. G22)	7	1064	2.6844×10^{-2}	0.9914×10^{-2} (59%)	3.13	0.847 (37%)
G01-G53**	Data-points with only $0.5 \leq e < 1$	Table 6 /S23	818	2.959×10^{-2}	1.266×10^{-2} (75%)	3.437	1.154 (51%)

(G_S) or the soil specific exponent on the e term, which would be difficult to determine a-priori without soil specific test data. Increased prediction accuracy potentially may be achieved using a calibrated form of Eq. (8) but knowledge of additional parameters would be needed.

In contrast to e, the pore size indicators (e.g., D_{10}, R_H, S_A) exhibit strong predictive strength for K in granular soils. However, for single test data series, e is crucial to the K variation. These findings are based on the available data from the studied database. However, due to the relatively large number of data sources (53 in total), some of the scatter shown may be from the inconsistency in the test methods and the inherent variability of the data from different sources as well as the need to assume the test temperature for some of the data records.

Declaration of Competing Interest

The authors declare that they have no known competing financial interests or personal relationships that could have appeared to influence the work reported in this paper.

Data availability

This research has not generated any new experimental data.

Acknowledgements

The first author was supported by the scholarship from China Scholarship Council (CSC) under the Grant CSC No. 201708060067 for the work presented in this paper.

Appendix A. Supplementary data

Supplementary data to this article can be found online at https://doi.org/10.1016/j.trgeo.2023.101026.

References

[1] Taylor DW. Fundamentals of Soil Mechanics. New York, NY: John Wiley & Sons; 1948.
[2] Chapuis RP. Predicting the saturated hydraulic conductivity of soils: A review. Bull Eng Geol Environ 2012;71(3):401–34. https://doi.org/10.1007/s10064-012-0418-7.
[3] Shafiee A. Permeability of compacted granule-clay mixtures. Eng Geol 2008;97(3–4):199–208. https://doi.org/10.1016/j.enggeo.2008.01.002.
[4] Feia S, Dupla JC, Ghabezloo S, et al. Experimental investigation of particle suspension injection and permeability impairment in porous media. Geomech Energy Environ 2015;3:24–39. https://doi.org/10.1016/j.gete.2015.07.001.
[5] Ören AH, Özdamar T. Hydraulic conductivity of compacted zeolites. Waste Manag Res 2013;31(6):634–40. https://doi.org/10.1177/0734242X13479434.
[6] Sivapullaiah PV, Sridharan A, Stalin VK. Hydraulic conductivity of bentonite-sand mixtures. Can Geotech J 2000;37(2):406–13. https://doi.org/10.1139/t99-120.
[7] Di Donna A, Loveridge F, Piemontese M, Barla M. The role of ground conditions on the heat exchange potential of energy walls. *Geomech Energy Environ*. 2021;25: [article no. 100199]. http://doi.org/10.1016/j.gete.2020.100199.
[8] Alyamani MS, Sen Z. Determination of Hydraulic Conductivity from Complete Grain-Size Distribution Curves. Ground Water 1993;31(4):551–5. https://doi.org/10.1111/j.1745-6584.1993.tb00587.x.

[9] Mbonimpa M, Aubertin M, Chapuis RP, Bussie B. Practical pedotransfer functions for estimating the saturated hydraulic conductivity. Geotech Geol Eng 2002;20:235–59. https://doi.org/10.1023/A:1016046214724.

[10] Zhou Z, Fu HL, Liu BC, Tan HH, Long WX. Orthogonal tests on permeability of soil-rock-mixture. Chinese J Geotech Eng 2006;28(9):1134–8.

[11] Yang B, Liu Y, Wan F, et al. Experimental Study on Influence of Particle-Size Distribution on Permeability Coefficient of Sand. J Southwest Jiaotong Univ 2016;51(5):856–61. https://doi.org/10.3969/j.issn.0258-2724.2016.05.006.

[12] O'Kelly BC, Nogal M. Determination of Soil Permeability Coefficient Following an Updated Grading Entropy Approach. Geotech Res 2020;7(1):58–70. https://doi.org/10.1680/jgere.19.00036.

[13] Díaz-Curiel J, Miguel MJ, Biosca B, Arévalo-Lomas L. New granulometric expressions for estimating permeability of granular drainages. Bull Eng Geol Environ 2022;81(10). https://doi.org/10.1007/s10064-022-02897-4 [article no. 397].

[14] Mujtaba H, Shimobe S, Farooq K, Rehman Z ur, Khalid U. Relating gradational parameters with hydraulic conductivity of sandy soils: a renewed attempt. *Arab J Geosci* 2021;14(18):[article no. 1920]. http://doi.org/10.1007/s12517-021-08281-y.

[15] Zhai Q, Ye W, Rahardjo H, Satyanaga A, Dai G, Zhao X. Theoretical method for the estimation of vapour conductivity for unsaturated soil. *Eng Geol*. 2021;295:[article no. 106447]. https://doi.org/10.1016/j.enggeo.2021.106447.

[16] Hazen A. In: Some physical properties of sands and gravels with special reference to their filtration. Boston, MA: Wright & Potter Printing; 1893. p. 539–56.

[17] Hazen A. The Filtration of Public Water Supplies. New York, NY: John Wiley & Sons; 1895.

[18] Hazen A. Discussion of "Dam on Sand Foundation" by A. C. Koenig. Trans Am Soc Civ Eng 1911;73:199–203.

[19] Shepherd RG. Correlations of Permeability and Grain Size. Groundwater 1989;27(5):633–8. https://doi.org/10.1111/j.1745-6584.1989.tb00476.x.

[20] Chapuis RP. Predicting the saturated hydraulic conductivity of sand and gravel using effective diameter and void ratio. Can Geotech J 2004;41(5):787–95. https://doi.org/10.1139/t04-022.

[21] Kozeny J. Über kapillare leitung des wassers im boden:(aufstieg, versickerung und anwendung auf die bewässerung). *Hölder-Pichler-Tempsky*. 1927. (in German).

[22] Carman PC. Fluid flow through granular beds. Trans Inst Chem Eng 1937;15:150–66.

[23] Carman PC. Permeability of saturated sands, soils and clays. J Agric Sci 1939;29(2):262–72. https://doi.org/10.1017/S0021859600051789.

[24] Carrier WD. Goodbye, Hazen; Hello, Kozeny-Carman. *J Geotech Geoenvironmental Eng* 2003;129(11):1054–6. https://doi.org/10.1061/(ASCE)1090-0241(2003)129:11(1054).

[25] Ozgumus T, Mobedi M, Ozkol U. Determination of Kozeny Constant Based on Porosity and Pore to Throat Size Ratio in Porous Medium with Rectangular Rods. Eng Appl Comput Fluid Mech 2014;8(2):308–18. https://doi.org/10.1080/19942060.2014.11015516.

[26] Feng S, Vardanega PJ. Correlation of the Hydraulic Conductivity of Fine-Grained Soils with Water Content Ratio Using a Database. Environ Geotech 2019;6(5):253–68. https://doi.org/10.1680/jenge.18.00166.

[27] Feng S, Vardanega PJ. A database of saturated hydraulic conductivity of fine-grained soils: probability density functions. Georisk 2019;13(4):255–61. https://doi.org/10.1080/17499518.2019.1652919.

[28] Farrar DM, Coleman JD. The Correlation of Surface Area with Other Properties of Nineteen British Clay Soils. J Soil Sci 1967;18(1):118–24. https://doi.org/10.1111/j.1365-2389.1967.tb01493.x.

[29] Muhunthan B. Liquid limit and surface area of clays. Géotechnique 1991;41(1):135–8. https://doi.org/10.1680/geot.1991.41.1.135.

[30] Sridharan A, Rao SM, Murthy NS. Liquid limit of kaolinitic soils. Géotechnique 1988;38(2):191–8. https://doi.org/10.1680/geot.1988.38.2.191.

[31] Feng S, Vardanega PJ, Ibraim E, Widyatmoko I, Ojum C. Permeability assessment of some granular mixtures. Géotechnique 2019;69(7):646–54. https://doi.org/10.1680/jgeot.17.T.039.

[32] Lőrincz J. Relationship between grading entropy and dry bulk density of granular soils. Period Polytech Civ Eng 1990;34(3):255–65.

[33] Singh VP. Entropy Theory in Hydraulic Engineering. Reston, VA: American Society of Civil Engineers; 2014.

[34] Feng S, Vardanega PJ, Ibraim E, et al. Discussion: Permeability assessment of some granular mixtures. Géotechnique 2020;70(9):845–7. https://doi.org/10.1680/jgeot.19.D.005.

[35] Feng S, Vardanega PJ, James M, Ibraim E. Studying hydraulic conductivity of asphalt concrete using a database. *Transp Eng*. 2021;3:[article no. 100040]. http://doi.org/10.1016/j.treng.2020.100040.

[36] Terzaghi K, Peck RB. Soil Mechanics in Engineering Practice. New York, NY: John Wiley & Sons; 1948.

[37] Bear J. Dynamics of Fluids in Porous Media. New York, NY: American Elsevier Publishing; 1972.

[38] Wood DM. Soil Mechanics: A One-Dimensional Introduction. Cambridge, UK: Cambridge University Press; 2009.

[39] Barr DW. Coefficient of Permeability Determined By Measurable Parameters. Ground Water 2001;39(3):356–61. https://doi.org/10.1111/j.1745-6584.2001.tb02318.x.

[40] Ren X, Zhao Y, Deng Q, Kang J, Li D, Wang D. A relation of hydraulic conductivity — void ratio for soils based on Kozeny-Carman equation. Eng Geol 2016;213:89–97. https://doi.org/10.1016/j.enggeo.2016.08.017.

[41] Nishiyama N, Yokoyama T. Permeability of porous media: Role of the critical pore size. J Geophys Res Solid Earth 2017;122(9):6955–71. https://doi.org/10.1002/2016JB013793.

[42] Vardanega PJ, Waters TJ. Analysis of Asphalt Concrete Permeability Data Using Representative Pore Size. J Mater Civ Eng 2011;23(2):169–76. https://doi.org/10.1061/(ASCE)MT.1943-5533.0000151.

[43] Mathavan GN, Viraraghavan T. Coalescence/filtration of an oil-in-water emulsion in a peat bed. Water Res 1992;26(1):91–8. https://doi.org/10.1016/0043-1354(92)90116-L.

[44] Li J, Gu Y. Coalescence of oil-in-water emulsions in fibrous and granular beds. Sep Purif Technol 2005;42(1):1–13. https://doi.org/10.1016/j.seppur.2004.05.006.

[45] Fair GM, Hatch LP. Fundamental Factors Governing the Streamline Flow of Water Through Sand. J Am Water Works Assoc 1933;25(11):1551–63. https://doi.org/10.1002/j.1551-8833.1933.tb18342.x.

[46] Comiti J, Renaud M. A new model for determining mean structure parameters of fixed beds from pressure drop measurements: application to beds packed with parallelepipedal particles. Chem Eng Sci 1989;44(7):1539–45. https://doi.org/10.1016/0009-2509(89)80031-4.

[47] Ghassemi A, Pak A. Pore scale study of permeability and tortuosity for flow through particulate media using Lattice Boltzmann method. Int J Numer Analytical Methods Geomech 2011;35(8):886–901. https://doi.org/10.1002/nag.932.

[48] Nguyen TT, Indraratna B. The role of particle shape on the hydraulic conductivity of granular soils captured through Kozeny-Carman approach. Géotechnique Lett 2020;10(3):1–15. https://doi.org/10.1680/jgele.20.00032.

[49] Katagiri J, Kimura S, Noda S. Significance of shape factor on permeability anisotropy of sand: representative elementary volume study for pore-scale analysis. Acta Geotech 2020;15(8):2195–203. https://doi.org/10.1007/s11440-020-00912-0.

[50] Chapuis RP, Aubertin M. On the use of the Kozeny-Carman equation to predict the hydraulic conductivity of soils. Can Geotech J 2003;40(3):616–28. https://doi.org/10.1139/t03-013.

[51] Baver LD. Soil Physics. New York, NY: John Wiley & Sons; 1948.

[52] Yokoyama T, Takeuchi S. Porosimetry of vesicular volcanic products by a water-expulsion method and the relationship of pore characteristics to permeability [article no. B02201] J Geophys Res Solid Earth 2009;114(2). https://doi.org/10.1029/2008JB005758.

[53] Lambe TW, Whitman RV. Soil Mechanics. New York, NY: John Wiley & Sons; 1969.

[54] Zhai Q, Rahardjo H, Satyanaga A. A pore-size distribution function based method for estimation of hydraulic properties of sandy soils. Eng Geol 2018;246:288–92. https://doi.org/10.1016/j.enggeo.2018.09.031.

[55] Zhai Q, Ye W, Rahardjo H, Satyanaga A, Du Y, Dai G, et al. Estimation of the hydraulic conductivity of unsaturated soil incorporated the film flow. Can Geotech J 2022;59(9):1679–84. https://doi.org/10.1139/cgj-2021-0361.

[56] Ren X, Santamarina JC. The hydraulic conductivity of sediments: A pore size perspective. Eng Geol 2018;233:48–54. https://doi.org/10.1016/j.enggeo.2017.11.022.

[57] Trani LDO, Indraratna B. The use of particle size distribution by surface area method in predicting the saturated hydraulic conductivity of graded granular soils. Géotechnique 2010;60(12):957–62. https://doi.org/10.1680/geot.9.T.014.

[58] Chapuis R, Légaré PP. A Simple Method for Determining the Surface Area of Fine Aggregates and Fillers in Bituminous Mixtures. In: Meininger RC, (ed.) *Effects of Aggregates and Mineral Fillers on Asphalt Mixture Performance*. ASTM STP 1147. West Conshohocken, PA: ASTM International; 1992:177-186. http://doi.org/10.1520/STP24217S.

[59] Phoon KK, Ching J, Wang Y. Managing Risk in Geotechnical Engineering – From Data to Digitalization. In: Ching J, Li DQ, Zhang J. (eds.) *Proceedings of the 7th International Symposium on Geotechnical Safety and Risk (ISGSR 2019)*. 2019:13-34. Available from: <https://www.issmge.org/uploads/publications/96/97/SL.pdf> [26/04/2023].

[60] Feng S. Hydraulic Conductivity of Road Construction Materials: with a focus on freeze-thaw effects. Bristol, UK: University of Bristol; 2022. Ph.D. thesis.

[61] Feng S, Vardanega PJ, Ibraim E. Comparison of Prediction Models for the Permeability of Granular Materials Using a Database. In: Hemeda S, Bouassida M. (eds.) *Contemporary Issues in Soil Mechanics*. Sustainable Civil Infrastructures. Springer; 2019:1-13. https://doi.org/10.1007/978-3-030-01941-9_1.

[62] Mavis FT, Wilsey EF. A Study of the Permeability of Sand. Iowa City, IA: University of Iowa; 1936. https://doi.org/10.17077/006163.

[63] Chu TY, Davidson DT, Wickstrom AE. Permeability Test for Sands. In: *Symposium on Permeability of Soils*. ASTM International; 1955:43-56. http://doi.org/10.1520/STP46164S.

[64] Dudgeon CR. An experimental study of the flow of water through coarse granular media. La Houille Blanche 1966;52(7):785–801. https://doi.org/10.1051/lhb/1966049.

[65] Morris D, Johnson A. *Summary of Hydrologic and Physical Properties of Rock and Soil Materials, as Analyzed by the Hydrologic Laboratory of the U.S. Geological Survey, 1948-1960*. Washington DC, USA: United States Department of the Interior; 1967. Available from: <https://pubs.usgs.gov/wsp/1839d/report.pdf> [26/04/2023].

[66] Bo M. Fundamentals of Flow through Packed Beds. Loughborough, UK: Loughborough University of Technology; 1968. Ph.D. thesis. Available from: <https://hdl.handle.net/2134/33595> [26/04/2023].

[67] Goetz RO. Investigation into Using Air in the Permeability Testing of Granular Soils. Ann Arbor, MI: University of Michigan; 1971. Final Report ORA Project 335130. Available from: <https://deepblue.lib.umich.edu/bitstream/hand

le/2027.42/5147/bac3009.0001.001.pdf?sequence=5&isAllowed=y> [26/04/2023].
[68] Moulton L, Seals D. Determination of the In Situ Permeability of Base and Subbase Courses. *Report No. FHWA-RD-79-88*. Washington DC, USA: Federal Highway Administration; 1979. Available from: <https://rosap.ntl.bts.gov/view/dot/30030/dot_30030_DS1.pdf> [26/04/2023].
[69] Shahabi A, Das B, Tarquin A. An Empirical Relation for Coefficient of Permeability of Sand. In: *Fourth Australia-New Zealand Conference on Geomechanics*. Perth, WA; 1984:54-57. Available from: <https://www.issmge.org/uploads/publications/89/91/4ANZ_008.pdf> [26/04/2023].
[70] Highlands KL, Hoffman GL. Subbase permeability and pavement performance. *Transp Res Rec*. 1988;(1159):7-20. Available from: <https://onlinepubs.trb.org/Onlinepubs/trr/1988/1159/1159-002.pdf> [26/04/2023].
[71] Rockhold ML, Fayer MJ, Gee CW. *Characterization of Unsaturated Hydraulic Conductivity at the Hanford Site*. Washington, USA: U.S. Department of Energy; 1988. https://doi.org/10.2172/6970088.
[72] Chapuis RP, Gill DE, Baass K. Laboratory permeability tests on sand: influence of the compaction method on anisotropy. Can Geotech J 1989;26(4):614–22. https://doi.org/10.1139/t89-074.
[73] Yeh T-C-J, Harvey DJ. Effective unsaturated hydraulic conductivity of layered sands. Water Resour Res 1990;26(6):1271–9. https://doi.org/10.1029/WR026i006p01271.
[74] Olanrewaju JN, Wong T-F. Hydraulic Conductivity, Porosity and Particle Size Distribution of Core Samples of the Upper Glacial Aquifer: Laboratory Observations. Stony Brook, NY: State University of New York at Stony Brook; 1994. Available from: <http://hdl.handle.net/11401/64889> [26/04/2023].
[75] Tangpithakkul R. Study of Permeability of Pavement Base Materials. Athens, OH: Ohio University; 1997. M.Sc. thesis, Available from: <https://etd.ohiolink.edu/apexprod/rws_etd/send_file/send?accession=ohiou1184344573&dispositionion=inline> [26/04/2023].
[76] Heindel and Noyes. Permeability of Highway Base and Sub-Base Material. Builington, VT: Vermont Agency of Transportation; 1997. Available from: <https://vtrans.vermont.gov/sites/aot/files/highway/documents/materialsandresearch/completedprojects/AOT_PermeabilityofHighwayBaseandSub-baseMaterial.pdf> [26/04/2023].
[77] Hatanaka M, Uchida A, Takehara N. Permeability Characteristics of High-Quality Undisturbed Sands Measured in A Triaxial Cell. Soils Found 1997;37(3):129–35. https://doi.org/10.3208/sandf.37.3_129.
[78] Yin J, Hachiya Y. Permeability of drainage base course materials at laboratory tests. J Pavement Eng 1998;3:175–82. https://doi.org/10.2208/journalpe.3.175.
[79] Tanaka T, Verruijt A, Hayashi K. Seepage failure experiments on sand behind sheet piles. In: Kusakabe O, Fujita K, Miyazaki Y. (eds.) *Geotechnical Aspects of Underground Construction in Soft Ground*. 2000:717-722. Available from: <https://www.issmge.org/uploads/publications/6/9/1999_115.pdf> [26/04/2023].
[80] Hatanaka M, Uchida A, Taya Y, et al. Permeability Characteristics of High-Quality Undisturbed Gravelly Soils Measured in Laboratory Tests. Soils Found 2001;41(3):45–55. https://doi.org/10.3208/sandf.41.3_45.
[81] Yang H, Rahardjo H, Leong EC, Fredlund DG. A study of infiltration on three sand capillary barriers. Can Geotech J 2004;41(4):629–43. https://doi.org/10.1139/T04-021.
[82] Rankine KJ. An Investigation into the Drainage Characteristics and Behaviour of Hydraulically Placed Mine Backfill and Permeable Minefill Barricades. Ph.D. thesis. Qld, Australia: James Cook University; 2005.
[83] Watabe Y, Saitoh K. Influence of sand fraction on compressibility and hydraulic conductivity of clayey soils. In: *Proceedings of the 16th International Conference on Soil Mechanics and Geotechnical Engineering*. IOS Press; 2005:615-618. http://doi.org/10.3233/978-1-61499-656-9-615.
[84] Indrawan IGB, Rahardjo H, Leong EC. Effects of coarse-grained materials on properties of residual soil. Eng Geol 2006;82(3):154–64. https://doi.org/10.1016/j.enggeo.2005.10.003.
[85] Bandini P, Sathiskumar S. Effects of Silt Content and Void Ratio on the Saturated Hydraulic Conductivity and Compressibility of Sand-Silt Mixtures. J Geotech Geoenvironmental Eng 2009;135(12):1976–80. https://doi.org/10.1061/(ASCE)GT.1943-5606.0000177.
[86] Khoury N, Zaman M, Ghabchi R, Kazmee H. Stability and Permeability of Proposed Aggregate Bases in Oklahoma, *Final Report - FHWA-OK-09-05*. Norman, OK: The University of Oklahoma; 2010. Available from: <https://www.odot.org/hqdiv/p-r-div/spr-rip/library/reports/rad_spr2-i2196-fy2009-rpt-final-zaman.pdf> [26/04/2023].
[87] Ghabchi R, Zaman M, Khoury N, Kazmee H, Solanki P. Effect of gradation and source properties on stability and drainability of aggregate bases: a laboratory and field study. Int J Pavement Eng 2013;14(3):274–90. https://doi.org/10.1080/10298436.2012.711475.
[88] Bouteldja F, Breul P, Boissier D. Experimental Validation of an Method for In Situ Estimation of Hydraulic Conductivity of Water Treatment Granular Materials. Geotech Geol Eng 2011;29(6):1009–21. https://doi.org/10.1007/s10706-011-9433-x.
[89] Santillan DY, Martin del Campo JJS. Filter ratio between materials in a rockfill dam. In: *Proceedings 2011 Pan-Am CGS Geotechnical Conference 64th Canadian Geotechnical Conference*. Toronto, ON; 2011. Available from: <https://www.issmge.org/uploads/publications/84/52/GEO11Paper830.pdf> [26/04/2023].
[90] Indraratna B, Nguyen VT, Rujikiatkamjorn C. Hydraulic conductivity of saturated granular soils determined using a constriction-based technique. Can Geotech J 2012;49(10):607–13. https://doi.org/10.1139/t2012-016.
[91] Dolzyk K, Chmielewska I. Predicting the Coefficient of Permeability of Non-Plastic Soils. Soil Mech Found Eng 2014;51(5):213–8. https://doi.org/10.1007/s11204-014-9279-3.
[92] Bin CX, Li ZY, Zhang JS. Effect of granite gravel content on improved granular mixtures as railway subgrade fillings. J Cent South Univ 2014;21(8):3361–9. https://doi.org/10.1007/s11771-014-2310-z.
[93] Cetin A, Kaya Z, Cetin B, Aydilek AH. Influence of laboratory compaction method on mechanical and hydraulic characteristics of unbound granular base materials. Road Mater Pavement Des 2014;15(1):220–35. https://doi.org/10.1080/14680629.2013.869505.
[94] Rosas J, Lopez O, Missimer TM, et al. Determination of hydraulic conductivity from grain-size distribution for different depositional environments. Groundwater 2014;52(3):399–413. https://doi.org/10.1111/gwat.12078.
[95] Jaafar R, Likos WJ. Pore-Scale Model for Estimating Saturated and Unsaturated Hydraulic Conductivity from Grain Size Distribution [article no. 04013012] J Geotech Geoenviron Eng 2014;140(2). https://doi.org/10.1061/(ASCE)GT.1943-5606.0001031.
[96] Cai J, Taute T, Hamann E, Schneider M. An Integrated Laboratory Method to Measure and Verify Directional Hydraulic Conductivity in Fine-to-Medium Sandy Sediments. Groundwater 2015;53(1):140–50. https://doi.org/10.1111/gwat.12156.
[97] Liu Y. Permeability and Pore Structure of Granular Materials. Hamilton, ON: McMaster University; 2015. Ph.D. thesis. Available from: <http://hdl.handle.net/11375/18104> [26/04/2023].
[98] Qiu ZF, Wang JJ. Experimental study on the anisotropic hydraulic conductivity of a sandstone-mudstone particle mixture [article no. 04015029] J Hydrol Eng 2015;20(11). https://doi.org/10.1061/(ASCE)HE.1943-5584.0001220.
[99] Nemes A, Schaap M, Leij FJ, Wösten JHM. *UNSODA 2.0: Unsaturated Soil Hydraulic Database. Database and Program for Indirect Methods of Estimating Unsaturated Hydraulic Properties*. USDA Agricultural Research Service; 2015. Available from: <https://data.nal.usda.gov/dataset/unsoda-20-unsaturated-soil-hydraulic-database-database-and-program-indirect-methods-estimating-unsaturated-hydraulic-properties> [26/04/2023].
[100] Cabalar AF, Akbulut N. Evaluation of actual and estimated hydraulic conductivity of sands with different gradation and shape [article no. 820] Springerplus 2016;5(1). https://doi.org/10.1186/s40064-016-2472-2.
[101] Wang X, Wang X, Chen J, Wang R, Hu M, Meng Q. Experimental study on permeability characteristics of calcareous soil. Bull Eng Geol Environ 2017;77(4):1753–62. https://doi.org/10.1007/s10064-017-1104-6.
[102] Feng S. Assessing the Permeability of Pavement Construction Materials by Using Grading Entropy Theory. M.Sc. thesis. Bristol, UK: University of Bristol; 2017.
[103] Mneina A, Shalaby A, Soliman H, Kass S. Effects of Unbound Granular Materials Gradation Parameters on the Drainage Quality of Pavement Structures. In: *TAC 2018: Innovation and Technology: Evolving Transportation-2018 Conference and Exhibition of the Transportation Association of Canada*. 2018. Available from: <https://www.tac-atc.ca/sites/default/files/conf_papers/mneinaa-effects_of_unbound.pdf> [26/04/2023].
[104] Chung CK, Kim JH, Kim J, Kim T. Hydraulic Conductivity Variation of Coarse-Fine Soil Mixture upon Mixing Ratio. *Adv Civ Eng*. 2018;2018:[article no. 6846584] https://doi.org/10.1155/2018/6846584.
[105] Bag R, Jadda K, Srikanth R. Effect of sand ratio on swelling pressure and hydraulic conductivity of an Indian bentonite-sand mixture. In: *Proc. 7th Int. Conf. on Unsaturated Soils (UNSAT2018)*. Hong Kong: CRC Press; 2018. Available from: <https://www.issmge.org/uploads/publications/62/63/5-3.UNSAT2018_354.pdf> [26/04/2023].
[106] Boley C, Forouzandeh Y, Wagner S. Fundamental research on penetration grouting with acrylates in porous media. In: Sigursteinsson H, Erlingsson S, Bessason B, editors. Proceedings of the XVII ECSMGE-2019: Geotechnical Engineering foundation of the future; 2019. https://doi.org/10.32075/17ECSMGE-2019-0634.
[107] Gao QF, Dong H, Huang R, Li ZF. Structural characteristics and hydraulic conductivity of an eluvial-colluvial gravelly soil. Bull Eng Geol Environ 2019;78(7):5011–28. https://doi.org/10.1007/s10064-018-01455-1.
[108] Dong H, Huang R, Gao QF. Rainfall infiltration performance and its relation to mesoscopic structural properties of a gravelly soil slope. Eng Geol 2017;230:1–10. https://doi.org/10.1016/j.enggeo.2017.09.005.
[109] Shamsuddin MKN, Sulaiman WNA, Ramli MF, Kusin FM. Vertical hydraulic conductivity of riverbank and hyporheic zone sediment at Muda River riverbank filtration site, Malaysia. *Appl Water Sci* 2019;9(1). https://doi.org/10.1007/s13201-018-0880-x [article no. 8].
[110] Taiba CA, Mahmoudi Y, Hazout L, Belkhatir M, Baille W. Evaluation of hydraulic conductivity through particle shape and packing density characteristics of sand–silt mixtures. Mar Georesources Geotechnol 2019;37(10):1175–87. https://doi.org/10.1080/1064119X.2018.1539891.
[111] Arshad M, Nazir MS, O'Kelly BC. Evolution of hydraulic conductivity models for sandy soils. Proc Inst Civ Eng - Geotech Eng 2020;173(2):97–114. https://doi.org/10.1680/jgeen.18.00062.
[112] Rees C, Palmer A, Palmer J, Singh R. Variation in Saturated Hydraulic Conductivity at the Outcrop Scale, the Whanganui Basin. New Zealand *Groundwater* 2020;58(4):622–37. https://doi.org/10.1111/gwat.12948.
[113] Toumpanou IC, Pantazopoulos IA, Markou IN, Atmatzidis DK. Predicted and measured hydraulic conductivity of sand-sized crushed limestone. Bull Eng Geol Environ 2021;80(2):1875–90. https://doi.org/10.1007/s10064-020-02032-1.
[114] Corey AT. Measurement of Water and Air Permeability in Unsaturated Soil. Soil Sci Soc Am J 1957;21(1):7–10. https://doi.org/10.2136/sssaj1957.03615995002100010003x.

[115] Jarque CM, Bera AK. Efficient tests for normality, homoscedasticity and serial independence of regression residuals. Econ Lett 1980;6(3):255–9. https://doi.org/10.1016/0165-1765(80)90024-5.
[116] Fernandez GCJ. Residual Analysis and Data Transformations: Important Tools in Statistical Analysis. HortSci 1992;27(4):297–300. http://doi.org/10.21273/hortsci.27.4.297.
[117] Montgomery DC, Runger GC, Hubele NF. Engineering Statistics. 4th ed. New York, NY: John Wiley & Son Inc; 2007.
[118] Velleman PF, Welsch RE. Efficient Computing of Regression Diagnostics. Am Stat 1981;35(4):234–42. https://doi.org/10.2307/2683296.
[119] Piñeiro G, Perelman S, Guerschman JP, Paruelo JM. How to evaluate models: Observed vs. predicted or predicted vs. observed? Ecol Modell 2008;216(3–4):316–22. https://doi.org/10.1016/j.ecolmodel.2008.05.006.
[120] Spiess AN, Neumeyer N. An evaluation of R^2 as an inadequate measure for nonlinear models in pharmacological and biochemical research: a Monte Carlo approach. BMC Pharmacol 2010;10(1). https://doi.org/10.1186/1471-2210-10-6 [article no. 6].
[121] Feng S, Vardanega PJ, Ibraim E, Barreto D, Imre E. The use of grading entropy for assessing granular soil hydraulic conductivity. *17th Asian Regional Conference on Soil Mechanics and Geotechnical Engineering*. 2023. accepted for publication.
[122] ASTM International. *Standard Practice for Classification of Soils for Engineering Purposes (Unified Soil Classification System)*. West Conshohocken, PA: ASTM International; 2017. https://doi.org/10.1520/D2487-11.
[123] Waters TJ, Vardanega PJ. Re-examination of the coefficient of determination (r^2) using road materials engineering case studies. Road Transp Res 2009;18(3):3–11.